AMPK-dependent phosphorylation of the GATOR2 component WDR24 suppresses glucose-mediated mTORC1 activation

Xiaoming Dai[1,6], **Cong Jiang**[1,6], **Qiwei Jiang**[2,6], **Lan Fang**[3], **Haihong Yu**[3], **Jinhe Guo**[2], **Peiqiang Yan**[1], **Fangtao Chi**[4], **Tao Zhang**[1], **Hiroyuki Inuzuka**[1], **John M. Asara**[5], **Ping Wang**[3], **Jianping Guo**[2,✉], **Wenyi Wei**[1,✉]

[1]Department of Pathology, Beth Israel Deaconess Medical Center, Harvard Medical School, Boston, MA, USA.

[2]Institute of Precision Medicine, the First Affiliated Hospital, Sun Yat-sen University, Guangzhou, China.

[3]Tongji University Cancer Center, Shanghai Tenth People's Hospital, School of Medicine, School of Life Sciences and Technology, Tongji University, Shanghai, China.

[4]The David H. Koch Institute for Integrative Cancer Research at Massachusetts Institute of Technology, Department of Biology, Massachusetts Institute of Technology, Cambridge, MA, USA.

[5]Division of Signal Transduction, Beth Israel Deaconess Medical Center and Department of Medicine, Harvard Medical School, Boston, MA, USA.

[6]These authors contributed equally: Xiaoming Dai, Cong Jiang, Qiwei Jiang.

Abstract

The mechanistic target of rapamycin complex 1 (mTORC1) controls cell growth in response to amino acid and glucose levels. However, how mTORC1 senses glucose availability to regulate various downstream signalling pathways remains largely elusive. Here we report that AMP-activated protein kinase (AMPK)-mediated phosphorylation of WDR24, a core component of the GATOR2 complex, has a role in the glucose-sensing capability of mTORC1.

Mechanistically, glucose deprivation activates AMPK, which directly phosphorylates WDR24 on S155, subsequently disrupting the integrity of the GATOR2 complex to suppress mTORC1 activation. Phosphomimetic $Wdr24^{S155D}$ knock-in mice exhibit early embryonic lethality and reduced mTORC1 activity. On the other hand, compared to wild-type littermates, phospho-deficient $Wdr24^{S155A}$ knock-in mice are more resistant to fasting and display elevated mTORC1 activity. Our findings reveal that AMPK-mediated phosphorylation of WDR24 modulates glucose-induced mTORC1 activation, thereby providing a rationale for targeting AMPK–WDR24 signalling to fine-tune mTORC1 activation as a potential therapeutic means to combat human diseases with aberrant activation of mTORC1 signalling including cancer.

Amino acids and glucose are two essential nutrient factors for organism survival[1–3]. Mechanistic target of rapamycin complex 1 (mTORC1) regulates cell growth and metabolism in response to amino acid and glucose availability[4,5]. Mechanistically, mTORC1 senses amino acids mainly through the GATOR1 and GATOR2 (GATOR1/2) complexes[6,7]. GATOR1 (DEPDC5, NPRL2 and NPRL3) functions as a GTPase-activating protein (GAP) towards RagA and RagB, while GATOR2, consisting of WDR24, Mios, WDR59, Seh1L and Sec13, inhibits GATOR1's GAP activity to activate mTORC1 with a yet unknown mechanism[6]. Notably, GATOR2 senses amino acids through different amino acid sensors such as Sestrin2 (ref. [8]), CASTOR1 (ref. [9]) and SAR1B[10]. Although there are implications that GATOR1/2 may also have a critical role in mTORC1 glucose sensing[11], it is largely unknown whether and how GATOR1/2 mediate mTORC1 glucose sensing.

As a key energy sensor[12–14], AMP-activated protein kinase (AMPK) has a critical role in mTORC1 inhibition in part through the phosphorylation of TSC2 (refs.[15,16]) and Raptor[16,17]. Although the ability to sense and adapt to amino acid and glucose availability is extremely important for cells to survive in various environments[1–3], whether and how amino acid sensing and glucose sensing are co-ordinately regulated remain largely unclear. Hence, it is worthwhile to investigate whether the amino acid-sensing machinery of GATOR1/2 complexes could have a role in mTORC1's capacity of sensing glucose and how this process probably cross-talks with the energy sensor AMPK.

Results

GATOR1/2 complexes modulate mTORC1 glucose sensing

When exploring the function of GATOR1/2 in sensing glucose availability by mTORC1, we found that depletion of the GATOR1 component *NPRL2* or *DEPDC5* led to sustained mTORC1 activation even under glucose deprivation (Fig. 1a,b and Extended Data Fig. 1a–c). On the other hand, in cells with genetic deficiency of the GATOR2 component *WDR24*, *WDR59* or *MIOS*, mTORC1 activation induced by glucose stimulation was largely compromised (Fig. 1c–e and Extended Data Fig. 1d–f). Furthermore, in *WDR24* knockout cells, reconstitution of wild-type (WT) WDR24 could rescue mTORC1 glucose sensing (Extended Data Fig. 1g). These results suggest that, as with their functions in sensing amino acids, GATOR1/2 complexes also have an essential role for mTORC1 in sensing glucose. This finding is consistent with previous reports[11,18,19] suggesting that the GATOR–Rag GTPase signalling axis functions in mTORC1 glucose sensing. However,

the phosphorylation status of TSC2 and Raptor, two previously reported substrates of AMPK[15,17], was comparably regulated by glucose availability in WT and GATOR1/2 component knockout cell lines (Fig. 1a–e and Extended Data Fig. 1a,d), indicating that the observed phenotypes in mTORC1 sensing of glucose are probably independent of AMPK-mediated phosphorylation of TSC2 or Raptor.

Lysosome recruitment of mTORC1 complex is a prerequisite for its activation, which is predominantly controlled by the GATOR–Rag GTPase pathway[6,20]. Consistent with these reports[6,20], glucose stimulation increased mTOR colocalization with the lysosome makers LAMP1 in WT cells (Fig. 1f–i and Extended Data Fig. 1h–k). However, mTOR consistently colocalized with lysosome in *NPRL2* knockout cells either with or without glucose stimulation (Fig. 1f,g and Extended Data Fig. 1h,i). Of note, the colocalization of mTOR with lysosome was not significantly increased after glucose stimulation in *WDR24* knockout cells (Fig. 1h,i and Extended Data Fig. 1j,k). These data together suggest that glucose availability controls mTORC1 lysosome localization and activation mainly through the GATOR1/2 complexes.

AMPK and GATOR1/2 co-ordinately regulate mTORC1 glucose sensing

As an energy sensor, AMPK has been established as a key regulator of mTORC1 activation under glucose stimulation[15,17,21]. In keeping with these reports[15,17,21], we found that loss of *AMPKα1/2* notably blocked glucose deprivation-induced mTORC1 inactivation (Extended Data Fig. 2a–d). Notably, reconstitution of AMPKα1 or α2 restored the suppression of mTORC1 by glucose starvation in *AMPKα1* and *AMPKα2* knockout cells (Extended Data Fig. 2d), thereby demonstrating a key role of AMPKα in this process. Due to the critical role of glucose in modulating mTOR lysosome localization (Fig. 1f–i and Extended Data Fig. 1h–k), we further investigated whether AMPK could regulate mTOR lysosome localization. To this end, although glucose could still promote mTOR lysosome localization in *AMPKα1/2* knockout cells[11], compared with the counterpart cells, mTOR was partially resistant to lysosome delocalization in *AMPKα1/2* knockout cells on glucose starvation (Fig. 2a,b). Furthermore, the AMPK-specific agonist A-769662 (ref. [22]) significantly suppressed mTOR lysosome localization under nutrient-rich conditions (Extended Data Fig. 2e,f), suggesting that AMPK regulates mTOR lysosome localization under energy-stressed conditions.

Because our data suggested that both GATOR1/2 complexes and AMPK have an important role in mTORC1 of sensing glucose and lysosome localization, it was intriguing to investigate whether AMPK and GATOR1/2 complexes co-ordinately regulate mTORC1 glucose sensing. To this end, we found that on additional depletion of *NPRL2* in *AMPKα1/2* knockout cells, mTORC1 exhibited high activity under glucose starvation (Fig. 2c), whereas in *AMPKα1/2* knockout cells with additional depletion of *WDR59*, mTORC1 activity remained at basal level on glucose stimulation (Fig. 2d). Moreover, based on the reported evidence that GATOR2 functions upstream of the GATOR1 complex[6,23], our results indicate that AMPK may function upstream of GATOR2 to govern mTORC1 activation by glucose availability.

AMPK interacts with WDR24 and phosphorylates it on S155

As a kinase, AMPK exerts its biological functions largely through phosphorylating diverse downstream substrates[12–14]. In support of the notion that AMPK can directly regulate GATOR2, we found that AMPKα1 interacted strongly with WDR24, WDR59 and Mios, and weakly with Seh1L and Sec13 in cells (Fig. 2e and Extended Data Fig. 3a–c), but the interaction was not obviously regulated by glucose availability (Extended Data Fig. 3d). Furthermore, the interaction between AMPKα1 and WDR59 or Mios was largely compromised in *WDR24* knockout cells (Fig. 2f) but not in *WDR59* or *MIOS* knockout cells (Extended Data Fig. 3e,f), suggesting that WDR24 may mediate the interaction between AMPK and the GATOR2 complex. Furthermore, the N-terminal WD40 domain of WDR24 was mapped to identify potential interactions with AMPK (Extended Data Fig. 3g,h). Meanwhile, the N-terminal kinase domain of AMPKα1 was observed to interact with WDR24 in cells (Extended Data Fig. 3i). Next, we explored whether AMPK could directly phosphorylate the GATOR2 components WDR24, WDR59, Mios, Seh1L and Sec13 by using an in vitro kinase assay. Of note, AMPK strongly phosphorylated only WDR24 but not the other components of GATOR2 including WDR59, Mios, Seh1L and Sec13 in vitro (Fig. 2g and Extended Data Fig. 3j). These results suggest that AMPK can directly regulate the function of the GATOR2 complex by phosphorylating WDR24.

Using the bioinformatics tool Scansite (https://scansite4.mit.edu) to predict the potential AMPK phosphorylation site, we found that only the WDR24-S155 site stood out with a high stringency standard (Extended Data Fig. 4a), which matched the optimal AMPK consensus motif LXRXXS/T[17,24] and was conserved across different species (Fig. 3a). High-resolution liquid chromatography–tandem mass spectrometry (LC–MS/MS) analyses further revealed that WDR24-S155 was phosphorylated in cells (Extended Data Fig. 4b). By contrast, substitution of S155 to alanine (S155A) largely diminished AMPK-mediated WDR24 phosphorylation in vitro (Fig. 3b). To further interrogate this phosphorylation in vivo, we developed and validated a phospho-specific antibody against WDR24-pS155 (Extended Data Fig. 4c,d) and observed that the S155A substitution markedly reduced the capacity of the developed antibody to recognize WDR24 (Extended Data Fig. 4d). Moreover, the antibody against WDR24-pS155 also recognized WDR24 phosphorylation in vitro (Extended Data Fig. 4e). Using the validated antibody against WDR24-pS155, we found that in keeping with our previous results, phosphorylation of WDR24 was markedly suppressed by glucose stimulation (Fig. 3c and Extended Data Fig. 4f) and administration of the AMPK inhibitor Compound C[25] (Extended Data Fig. 4g). On the other hand, phosphorylation of WDR24-S155 could be induced by the AMPK-specific agonist A-769662 (ref. [22]) or 991 (ref. [26]) (Fig. 3d). More importantly, glucose starvation-induced WDR24-S155 phosphorylation was largely abolished on *AMPKα1/2* deletion (Fig. 3e and Extended Data Fig. 4h). However, mutation of the WDR24-S155 site did not significantly affect the interaction between WDR24 and AMPKα1 (Extended Data Fig. 4i), indicating that glucose availability regulates GATOR2 by dictating the activity of AMPK. Although it is unclear whether other kinases might also phosphorylate WDR24 on the S155 site, our results demonstrate that WDR24 is indeed a bona fide downstream substrate of AMPK, at least in our experimental setting.

WDR24 phosphorylation inhibits mTORC1 activation

To further investigate the biological function of WDR24 phosphorylation by AMPK, we reconstituted *WDR24* knockout cells with WT WDR24, phospho-deficient mutant S155A or phosphomimetic mutant S155D. Notably, compared with WT WDR24-reconstituted cells, glucose stimulation could no longer activate mTORC1 in WDR24-S155D-reconstituted cells (Fig. 4a and Extended Data Fig. 5a). On the other hand, mTORC1 activity was relatively resistant to glucose starvation in the cells bearing WDR24-S155A (Fig. 4a and Extended Data Fig. 5a). These results suggest that phosphorylation of WDR24 at S155 inhibits the timely activation of mTORC1 induced by glucose stimulation.

In keeping with the critical role of mTORC1 in cell size control and an observed reduction of mTORC1 kinase activity in WRD24-S155D-rescued cells (Fig. 4a and Extended Data Fig. 5a), WDR24-S155D reconstituted cells were relatively smaller in size than WT WDR24 reconstituted cells (Fig. 4b and Extended Data Fig. 5b). Furthermore, reconstitution of WDR24-S155D also resulted in decreased cellular colony formation (Fig. 4c and Extended Data Fig. 5c). These data further confirm that AMPK-mediated WDR24-S155 phosphorylation suppresses mTORC1 activation in cells. Moreover, in keeping with the notion that both amino acids and glucose are essential for full activation of mTORC1[5,15,27], we found that under glucose starvation, amino acids alone could not fully activate mTORC1 (Extended Data Fig. 5d). Because the GATOR2 complex has a key role in amino acid-induced mTORC1 activation[6], we further tested whether WDR24-S155 phosphorylation could impact amino acid-induced mTORC1 activation. Interestingly, compared with WT WDR24-reconstituted cells, amino acids could not activate mTORC1 in WDR24-S155D-reconstituted cells (Extended Data Fig. 5e,f). These results explain the previous observations (Extended Data Fig. 5d) that amino acids cannot fully activate mTORC1 under glucose starvation[5,15,27]. In further support of the notion that AMPK has an important role in mTORC1 amino acid sensing, we found that under energy-rich conditions, AMPK was incapable of regulating mTORC1 amino acid sensing (Extended Data Fig. 5g,h)[18], while AMPK could potently inhibit mTORC1 amino acid sensing under glucose starvation (Extended Data Fig. 5g,h). These data suggest that under normal and glucose-rich culturing conditions, AMPK does not regulate mTORC1 amino acid sensing, whereas under energy-stressed conditions such as glucose starvation, AMPK could phosphorylate WDR24 to block mTORC1 amino acid sensing (Extended Data Fig. 5i).

To better understand the biological function of AMPK-mediated WDR24-S155 phosphorylation, we further generated *WDR24-S155D* knock-in HEK 293 cell lines using the CRISPR–Cas9 genome editing technology (Extended Data Fig. 6a–c). Notably, HEK 293 cells harbouring the S155D mutation displayed a dramatic reduction in glucose- and amino acid-induced mTORC1 activation (Fig. 4d and Extended Data Fig. 6d), which was consistent with the results obtained from the reconstituted *WDR24* knockout reconstituted cells (Fig. 4a and Extended Data Fig. 5a). Furthermore, the WDR24-S155D mutation also suppressed glucose- and amino acid-induced mTOR lysosome localization and cell growth (Fig. 4e,f and Extended Data Fig. 6e–g). Moreover, impaired mTORC1 activation in WDR24-S155D-expressing cells was largely prevented by ectopic expression of a constitutively active form of Rag GTPase (RagA-Q66L/RagC-S75N) (Extended Data Fig.

6h). Taken together, these results suggest that AMPK-mediated phosphorylation of WDR24-S155 impairs mTORC1's glucose- and amino acid-sensing abilities.

WDR24 phosphorylation regulates GATOR2 complex integrity

When further exploring the underlying mechanism, we observed that the S155D substitution of WDR24 markedly blocked its interaction with other GATOR2 components (Fig. 5a,b). These results suggest that the addition of a phosphate group on S155 may represent a local gain of function, which changes the conformation and subsequently blocks the interaction between WDR24 and other GATOR2 components. In support of this notion, glucose stimulation increased the interaction between WDR24 and WDR59 coupled with decreased WDR24-S155 phosphorylation (Fig. 5c and Extended Data Fig. 7a) and increased the GATOR2 integrity as shown by size-exclusion chromatography analyses (Extended Data Fig. 7b). On the other hand, consistent with previous reports[6,19,28], amino acid stimulation did not obviously regulate the interaction between WDR24 and WDR59 (Extended Data Fig. 7c,d) with a mild change of WDR24-S155 phosphorylation on amino acid stimulation (Extended Data Fig. 7d). Because AMPK only blocked mTORC1 amino acid sensing in energy-stressed (for example, glucose starvation) instead of normal (for example, glucose-rich) cell culturing conditions (Extended Data Fig. 5g–i), we further examined the interaction between WDR24 and other GATOR2 components under energy-stressed conditions, finding that such interactions were noticeably repressed (Extended Data Fig. 7e). When we further explored whether AMPK-mediated phosphorylation of WDR24 regulates GATOR2 integrity, we found that the S155D substitution of WDR24 could block glucose stimulation-induced interaction between WDR24 and WDR59 (Fig. 5d and Extended Data Fig. 7f). On the other hand, the S155A mutant maintained the interaction of WDR24 and WDR59 even after glucose starvation (Extended Data Fig. 7g). Consistent with this, the interaction between WDR24 and WDR59 was relatively more resistant to glucose starvation in *AMPKa1/2* knockout cells (Fig. 5e).

In keeping with the notion that AMPK-mediated phosphorylation of WDR24 probably creates a possible 14-3-3-binding epitope[29], we found that WDR24 specifically bound 14-3-3γ (Fig. 5f). More importantly, mTORC1 activity was relatively resistant to glucose starvation in *YWHAG* (*14-3-3γ*)-depleted cells (Fig. 5g). Interestingly, WDR24-S155D strongly interacted with 14-3-3γ more strongly than the WT and S155A mutant versions of WDR24 (Extended Data Fig. 7h). Moreover, glucose starvation could induce the interaction between 14-3-3γ and WT WDR24, but not the S155A mutant form of WDR24 (Fig. 5h,i). Thus, the interaction between WDR24 and WDR59 was relatively resistant to glucose starvation in *14-3-3γ*-depleted cells (Extended Data Fig. 7i). These data suggest that AMPK-mediated WDR24-S155 phosphorylation probably suppresses the formation of GATOR2 complex by recruiting 14-3-3 protein. Based on the structure of the GATOR2 complex[30], the WDR24 WD40 domain seems to mediate an interaction with the leucine sensor SESN2 (refs. [8,30]). Hence, we further investigated whether AMPK-mediated phosphorylation affected the interaction between SESN2 and WDR24. Notably, we found that the S155D substitution blocked the interaction with SESN2 (Extended Data Fig. 7j). Because both WDR24 and Seh1L are required for SESN2 interaction with GATOR2 (ref. [30]), the S155D mutation may block WDR24's interaction with SESN2 by disrupting the

integrity of the GATOR2 complex (Extended Data Fig. 7j). When we further tested whether SESN2 mediates mTORC1 glucose sensing, we found that although mTORC1 was relatively resistant to amino acid deprivation in *Sesn1*, *Sesn2* and *Sesn3* (*Sesn1/2/3*) triple knockout mouse embryonic fibroblasts (MEFs) (Extended Data Fig. 7k), mTORC1 could still respond to glucose starvation (Extended Data Fig. 7l). These results suggest that SESN2 may not be a major player in the mTORC1 glucose sensing process.

Homozygous *Wdr24*^S155D knock-in mice is lethal with lower mTORC1 activity

To better understand the physiological function of the AMPK-mediated phosphorylation of WDR24 in vivo, we generated phosphomimetic *Wdr24*^S155D knock-in mice (*Wdr24*^D/D) in a C57BL/6J background using the CRISPR–Cas9 technology (Extended Data Fig. 8a,b). While the heterozygous *Wdr24*^+/D mice were viable, no mice of homozygous *Wdr24*^D/D mice were born (Fig. 6a). Further characterization showed that *Wdr24*^D/D led to early embryonic lethality around embryonic day 10.5 and resulted in severely decreased body size (Fig. 6b), which resembled the phenotypes of *Rraga* (*RagA*)-deficient mice[31]. Consistent with the key role of WDR24-S155 phosphorylation in cells (Fig. 4a and Extended Data Fig. 5a), compared with WT counterpart mice, mTORC1 kinase activity was dramatically reduced in *Wdr24*^D/D mice as examined by the phosphorylation of S6 in foetal tissues (Fig. 6c). These results suggest that WDR24-S155 phosphorylation inhibits mTORC1 kinase activity in mice and further reveal a critical role of glucose sensing in embryonic development.

Wdr24^S155A mice exhibit high mTORC1 activity under fasting

With a similar approach, we generated phospho-deficient *Wdr24-S155A* mice (*Wdr24*^A/A) (Extended Data Fig. 8a,c). *Wdr24*^A/A mice were born at the expected Mendelian ratio with no obvious gross abnormality (Extended Data Fig. 8d). As anticipated, compared with WT mice, mTORC1 kinase activity was relatively higher in *Wdr24*^A/A knock-in mice after fasting (Fig. 6d,e and Extended Data Fig. 9a–f). To further explore the physiological role of WDR24-S155 phosphorylation in mTORC1 glucose sensing, we established MEFs from *Wdr24*^A/A mice. Compared with WT MEFs, mTORC1 was relatively resistant to glucose starvation in *Wdr24*^A/A MEFs (Fig. 6f). However, no obvious difference was observed in WT versus *Wdr24*^A/A MEFs in response to amino acid starvation (Extended Data Fig. 10a), which was consistent with our previous data (Extended Data Fig. 5e,f). Moreover, mTOR in *Wdr24*^A/A MEFs was consistently localized with lysosome under glucose starvation conditions (Extended Data Fig. 10b,c), while amino acids could still comparably regulate mTOR translocation to the lysosome (Extended Data Fig. 10d,e). These data further confirm that AMPK-mediated WDR24-S155 phosphorylation is necessary for mTORC1 activation in response to glucose availability in vivo.

Discussion

As a major requirement for biological life, glucose is constantly sensed by the mTORC1 pathway to regulate anabolic processes[27,32]. Understanding how mTORC1 senses glucose availability is not only important to better dissect the biological functions of mTOR, but also pivotal to develop potential therapeutic strategies for treating diseases characterized by

deregulated glucose availability, such as diabetes and cancer. mTORC1 can be regulated by glucose through AMPK-dependent and AMPK-independent mechanisms[33]. On the one hand, the energy sensor AMPK has been proposed to regulate mTORC1 by phosphorylating TSC2 (refs. [15,16]) and Raptor[16,17]. On the other hand, for AMPK-independent mechanisms, glucose availability influences several glycolytic intermediates such as glyceraldehyde-3-phosphate, fructose-1,6-bisphosphate, dihydroxyacetone phosphate and their cognate enzymes to regulate mTORC1 (refs.[11,34–37]). However, amino acids, another key building block of organisms and potent activators of mTORC1, are mainly sensed by mTORC1 through the GATOR–Rag GTPase axis[7]. Interestingly, the amino acid-sensing GATOR–Rag GTPase pathway has been implicated as having a role in mTORC1 glucose sensing[11,18,19], but the underlying mechanisms remain elusive. In this study, we showed that the amino acid sensing machinery GATOR1/2 complexes and energy sensor AMPK work in the same pathway to regulate mTORC1 glucose sensing. Mechanistically, AMPK phosphorylates WDR24 to inhibit the integrity of the GATOR2 complex, leading to the inhibition of mTORC1 kinase activity. These findings provide a new molecular mechanism whereby AMPK-mediated phosphorylation of WDR24 modulates mTORC1 glucose sensing (Fig. 6g). Taken together with previous reports[15,17], the findings reported in this article suggest that energy stress-induced AMPK activation directly phosphorylates TSC2, Raptor and WDR24 to ensure timely inhibition of mTORC1 activity through a three-pronged mechanism (Extended Data Fig. 10f).

More importantly, genetic mutation of the WDR24-S155 site to phosphomimetic S155D impairs the activation of mTORC1 kinase, leading to severe growth defects and early embryonic lethality in mice. Conversely, phospho-deficient $Wdr24^{S155A}$ knock-in mice are more resistant to fasting and display elevated mTORC1 activity. Taken together, our findings reveal that AMPK-mediated phosphorylation of WDR24 dictates glucose-mediated mTORC1 activation, thereby providing the rationale for targeting the AMPK–WDR24 signalling axis to control aberrant mTORC1 activation under different pathological conditions such as cancer.

Although we and others have reported that AMPK has important roles in mTORC1 glucose sensing by phosphorylating WDR24, Raptor and TSC2, it is worth noting that judging from the phenotypes of GATOR1/2 component knockout cells (Fig. 1 and Extended Data Fig. 1) and $Wdr24^{S155A/D}$ and $Wdr24^{S155D}$ knock-in cells and mice (Fig. 6 and Extended Data Figs. 9 and 10), GATOR1/2 complexes probably have a relatively more profound effect in mTORC1 glucose sensing than AMPK. Hence, apart from AMPK, whether other kinases or enzymes are also involved in regulating GATOR1/2 to mediate mTORC1 glucose sensing warrants further in-depth investigations. Notably, from the published elegant structure of the GATOR2 complex, it is obvious that although the WD40 domain of WDR24 does not directly mediate GATOR2 complex protein interaction[30], the location and the conformation surrounding the S155 site provide possible space for AMPK-mediated phosphorylation and the spatial need for the interaction with the 14-3-3γ protein to regulate the subsequent conformational change to impact the integrity of the GATOR2 complex. Although we cannot predict how this phosphorylation regulates the conformational change(s) of the GATOR2 complex, additional in-depth studies of cryogenic electron microscopy structures of GATOR2 containing WDR24-S155A versus WRD24-S155D or WDR24-S155 versus

WDR24-p155 are needed for further analyses. To this end, it will be ideal to compare the cryogenic electron microscopy structure of GATOR2 without S155 phosphorylation head to head with that of GATOR2 with phosphorylation at S155 under glucose starvation to reveal the conformational changes caused by WDR24 phosphorylation at S155. These findings will ultimately help us to better understand the detailed mechanisms of WDR24 phosphorylation and its potential impact on the integrity of GATOR2 and the regulation of mTORC1 signalling.

Methods

Cell culture, transfection and viral infection

No cell line used in this study is on the list of known misidentified cell lines maintained by the International Cell Line Authentication Committee (https://iclac.org/databases/cross-contaminations/). HEK 293, HEK 293T, HeLa, MEF and U2OS cells were maintained in Dulbecco's Modified Eagle Medium (DMEM) containing 10% fetal calf serum (FCS) (Gibco), 100 U ml^{-1} penicillin and 100 μg ml^{-1} streptomycin (Gibco). WT and *Ampkα1/2*$^{-/-}$ MEFs were kindly gifted by B. Viollet (Institut Cochin). WT and *AMPKα1/2*$^{-/-}$ U2OS cells were kindly gifted by R. Shaw's laboratory (Salk Institute). WT and *AMPKα1/2*$^{-/-}$ HEK 293T cells were kindly gifted by D. M. Sabatini's laboratory (Massachusetts Institute of Technology). WT and *Sesn1/2/3*$^{-/-}$ MEFs were kindly gifted by M. Li's laboratory (Memorial Sloan Kettering Cancer Center).

Transfection with polyethylenimine (Polysciences) or Lipofectamine (Invitrogen) was performed according to the manufacturer's instructions. To generate reconstituted cells, HEK 293T cells were transfected with viral constructs and the packaging plasmids. After 48 h of transfection, the viral supernatant was filtered through a filter (0.45 μm) and subsequently used to infect target cells supplemented with polybrene (4 μg ml^{-1}). Infected cells were selected with puromycin (1 μg ml^{-1}) or hygromycin B (200 μg ml^{-1}) as indicated for 3 d to eliminate non-infected cells.

Glucose/amino acid starvation and stimulation

For the glucose starvation and stimulation assay, cells were washed twice with PBS and then incubated in DMEM without glucose (Gibco) containing 10% dialysed FCS (Gibco), 100 μg ml^{-1} streptomycin and 100 IU penicillin for 1 h. Subsequently, cells were stimulated by adding glucose (25 mM) for the indicated times.

For the amino acid starvation and stimulation assay, experiments were performed as described previously[6]. Briefly, cells were rinsed twice with PBS and then incubated in amino acid-free RPMI 1640 supplemented with 10% dialysed FCS (Gibco) for 60 min. Cells were stimulated with amino acids for 10 min. The final concentration of amino acids was the same as in the RPMI 1640 medium.

Immunofluorescence staining

Cells were seeded on gelatin-coated coverslips in 24-well plates. After 24 h of seeding, the coverslips were washed with ice-cold PBS and fixed with 4% paraformaldehyde for 15 min

at room temperature. The resulting cells were then permeabilized with 0.05% Triton X-100 for 15 min. Permeabilized cells were incubated with 3% BSA in PBS for 1 h. Then, the slides were incubated with the indicated primary antibodies overnight at 4 °C, followed by incubation with the indicated secondary antibodies for 1–2 h. Images were acquired on a ZEISS LSM 510 META confocal system and Olympus FV1200 Laser Scanning Confocal Microscope. Microscopic images were collected with the ZEN 2012 microscopy software and Olympus FluoView, respectively. For quantitative analysis, images were analysed with ImageJ v.1.53a; approximately 15–30 cells were quantified with Pearson's correlation using the JACoP plugins.

Flow cytometry analysis of cell size

To determine cell size, HEK 293 or HeLa cells were seeded on 10-cm dishes at 40% confluence. After 24 h, cells were detached by trypsin and collected. Then, cells were washed with PBS and filtered with a 70-μm cell filter. The resulting cells were subjected to flow cytometry analysis. Cell size was indicated by forward scatter intensity.

Colony formation assays

HEK 293 or HeLa cells were plated in six-well plates with 800 cells per well and left for 8–10 d. The culture medium was changed every 2 d. When colonies grew to visible size, they were washed with PBS and then fixed with 10% acetic acid in 10% methanol for 15 min. The fixed colonies were then stained with 0.4% crystal violet in 20% ethanol for 15 min. After staining, the plates were gently washed with distilled water and air-dried. Colony numbers were counted and quantified.

Reagents

A-769662 (cat. no. S2697) and dorsomorphin (Compound C) (cat. no. S7306) were purchased from Selleck Chemicals. Glucose (cat. no. D9434) was purchased from Sigma-Aldrich and AMPK ($\alpha1/\beta1/\gamma2$) kinase (cat. no. P55-10H-10) was purchased from SignalChem Biotech. ATP-γ-S (cat. no. ab138911) and p-nitrobenzyl mesylate (cat. no. ab138910) were purchased from Abcam. Amino acid-free medium (cat. no. R8999-04A) was obtained from US Biological Life Sciences. DMEM without glucose (cat. no. 11966025), DMEM (cat. no. 11965092), FCS (cat. no. 16000044) and dialysed FCS (cat. no. 26400044) were purchased from Gibco.

MS analysis of WDR24-S155 phosphorylation

WDR24 knockout HEK 293 cells were reconstituted with lentiviral vectors expressing FLAG–WDR24. The resulting cells were collected to perform FLAG immunoprecipitation (IP). Briefly, samples were resolved by SDS–PAGE and the FLAG–WDR24 band was excised and analysed by MS as reported previously[38]. Fragmentation spectra were searched against the concatenated decoy human protein database v.20210315 (UniProt) using the Mascot 2.7 search engine. Data were interpreted and reported using the Scaffold Q+S 5.0 software (Proteome Software). Data-independent acquisition on the QExactive HF was also used to target and identify the doubly charged phosphorylated peptide

KDpSVSTFSGQSESVR ($(M + H)^{2+}$, *m/z* 847.88). Peptides were accepted if they passed a 1.0% false discovery rate threshold.

Plasmid construction

The pRK5-HA-WDR24 (46335), pLJM1-Flag-WDR24 (46337), pRK5-HA-Mios (46329), pRK5-HA-WDR59 (46328), pRK5-HA-Sec13 (46332) and pRK5-HA-Seh1L (46331) plasmids were obtained from Addgene. The pGEX-GST-6P2-WDR24 truncations were generated by subcloning the corresponding complementary DNAs into the pGEX-GST-6P2 vector.

For point mutations, different constructs were mutated using the QuikChange XL Site-Directed Mutagenesis Kit (Stratagene) according to the manufacturer's instructions.

Generation of the knockout cell lines

To generate the knockout cell lines, single-guide RNAs (sgRNAs) were cloned into the lentiCRISPR v2 Puro vector (cat. no. 52961, Addgene). After transfection with the indicated sgRNA for 24 h, cells were selected with puromycin for 2–3 d to eliminate the non-transfected cells. After selection, cells were plated in a 96-well plate. After 10–14 d, single clones were expanded, and the gene knockout event was verified via immunoblotting (IB) using the respective antibody. The sgRNA targeting sequences for WDR24, WDR59, Mios, DEPDC5 and NPRL2 (refs.[19,28]) and the sgRNA targeting sequences for AMPKα1 and AMPKα2 (ref. [39]) were described and validated previously.

Cell lysis

Cells were rinsed once with ice-cold PBS and then lysed with EBC buffer (0.5% NP-40, 120 mM NaCl, 50 mM Tris, pH 7.5, phosphatase inhibitors (Calbiochem) and protease inhibitors (Roche)). The cell lysates were centrifuged at 12,000 g for 10 min at 4 °C. Subsequently, the supernatant was transferred into a new microcentrifuge tube and the concentration was measured using the Bio-Rad protein assay reagent with a Beckman Coulter DU 800 spectrophotometer.

IP analysis

For the IP analysis, 1 mg total supernatant was incubated with haemagglutinin (HA)-agarose (cat. no. A-2095, Sigma-Aldrich) or FLAG-agarose (cat. no. A-2220, Sigma-Aldrich) for 2–3 h at 4 °C with rotation. Then, the beads were washed four times with NETN buffer (0.5% NP-40, 1 mM EDTA, 100 mM NaCl and 20 mM Tris, pH 8.0). Afterwards, the immunoprecipitates were denatured with SDS sample buffer and boiling for 5 min before being resolved by SDS–PAGE and analysed by IB with the indicated antibodies.

IB analysis

For the IB analysis, immunoprecipitates or whole-cell lysates (WCLs) were first resolved by 8–15% SDS–PAGE in SDS running buffer (25 mM Tris, pH 8.0, 200 mM glycine, 1% SDS). Subsequently, proteins were transferred to polyvinylidene difluoride membrane in transfer buffer (25 mM Tris, pH 8.0, 200 mM glycine, 20% methanol). Then, the membrane was incubated in blocking solution (5% milk, 20 mM Tris, pH 8.0, 150 mM NaCl, 0.1%

Tween 20) for 1 h at room temperature. The blocked membrane was incubated with the indicated primary antibodies at 4 °C overnight. Then, the membrane was washed three times in Tris-buffered saline with 0.1% Tween 20 (TBST) detergent buffer (20 mM Tris, pH 8.0, 150 mM NaCl, 0.1% Tween 20) at room temperature for 10 min on a shaker. After that, the membrane was incubated with the indicated secondary antibody for 1.5 h at room temperature. The membrane was washed three times with TBST buffer before developing the film. IB images were collected with the Epson Scan (v.3.9.3.0US) and quantified with ImageJ v.1.53a. The antibodies used in this study are listed in Supplementary Table 1. Key blots are quantified in Supplementary Table 3.

In vitro kinase assays

The AMPK in vitro kinase assays were performed as described previously[39]. Briefly, glutathione-S-transferase (GST)-tagged proteins (0.5 μg) purified from *Escherichia coli* were mixed with recombinant AMPK α1/β1/γ2 proteins (SignalChem) in the presence of 500 μM ATP-γ-S in AMPK kinase reaction buffer (SignalChem). The reaction mixtures were incubated for 30 min at 30 °C and then terminated by adding EDTA (20 μM). The mixtures were further supplied with 2.5 mM *p*-nitrobenzyl mesylate and incubated for 1 h at room temperature. The resulting samples were subjected to IB analysis.

Preparation of GST-tagged recombinant proteins

BL-21 competent cells were transformed with pGEX-GST-6P2 constructs expressing the indicated genes. Cells were grown at 37 °C to an optical density of 0.5–0.7. Protein production was induced by using 0.1 mM isopropyl β-D-1-thiogalactopyranoside at 18 °C overnight. Cells were collected by centrifugation and suspended in PBS containing protease inhibitor (Complete Mini, Roche). Then, cells were lysed by ultrasonication and centrifuged at 12,000 g for 15 min. The resulting supernatant was collected and incubated with glutathione beads (GE Healthcare) for 2–3 h at 4 °C. The glutathione beads were washed four times with PBS and eluted with elution buffer (10 mM GSH, 50 mM Tris-HCl, pH8.0, 150 mM NaCl).

Size-exclusion chromatography

The size-exclusion chromatography procedure was described previously[28,40]. Briefly, cells were rinsed once with ice-cold PBS buffer and then lysed in lysis buffer (50 mM HEPES, pH 7.4, 150 mM NaCl, 2.5 mM $MgCl_2$, 1% Triton X-100, 10% glycerolandprotein inhibitorcocktail). After centrifugation at 12,000 g for 30 min, 3 mg ofcelllysate was filtered with a 0.22-μM filter and loaded on a Superose 6 Increase 10/300 GL Column (GE Healthcare) connected to an AKTA purifier (GE Healthcare); 300-μl fractions were collected for each tube and subjected to SDS–PAGE.

Generation of *WDR24-S155D* knock-in HEK 293 cells

To generate the *WDR24-S155D* knock-in HEK 293 cells, the sgRNAs targeting the genomic sequence near the WDR24-S155 site were cloned into lentiCRISPR v2 GFP (cat. no. 82416, Addgene). The single-stranded oligodeoxynucleotide (ssODN) repair template was designed as reported previously[38] with the S155D mutation and a silent mutation to remove a BslI

restriction enzyme site. The GFP-sgRNA plasmids and the ssODN were cotransfected into HEK 293 cells. After 48 h, the GFP-positive cells were sorted by flow cytometry and plated into 96-well plates at one cell per well. After 10–14 d, visible single clones were transferred into 24-well plates. When cells increased in number, genomic DNA was extracted using the Quick Extract DNA extraction solution (cat. no. Q09050, Epicenter), subsequently amplified by PCR and digested by BslI (cat. no. R0555L, New England Biolabs). The *WDR24-S155D* knock-in cells were verified by Sanger sequencing. The primers and single-stranded DNA used for the generation of the knock-in cells are listed in Supplementary Table 2.

Generation of *Wdr24*[S155A] and *Wdr24*[S155D] mice

All the mice were maintained under appropriate conditions and subject to the ethical protocol approved by the Institutional Animal Care and Use Committee (IACUC) of Tongji University and Sun Yat-sen University. Eight-week-old C57BL/6 male and female mice were purchased from Shanghai Laboratory Animal Center. To generate the *Wdr24*[S155A] and *Wdr24*[S155D] mice, guide RNA targeting the *Wdr24* locus in exon 1, Cas9 mRNA and ssODN were mixed and co-microinjected into C57BL/6 mouse-derived zygotes. The *Wdr24*[S155A] and *Wdr24*[S155D] mice were verified by PCR. The primers and single-stranded DNA used to generate the knock-in mice are listed in Supplementary Table 2.

Mouse fasting experiment

The animal experiments were performed in accordance with a protocol approved by the IACUC of Tongji University and Sun Yat-sen University. Six-week-old C57/BL6 WT or *Wdr24*[S155A] male mice were randomly assigned to the fasting and fasting–refed groups. Each group used three mice. Mice were first fasted for 24 h and then fasted (fasting group) or fed (fasting–refed group) for 2 h. Mice were housed in specific pathogen-free facilities with a 12 h dark–light cycle under 21 °C and 50–60% humidity.

Embryo images and histological analysis

Embryos at different days of embryonic development were collected and imaged with an Olympus SZ61 microscope. For haematoxylin and eosin (H&E) staining, embryos were subsequently fixed in 4% paraformaldehyde and 4-μm sections were stained with H&E. For histological staining, pS6 (S240/244) was stained as reported previously[38].

Statistics and reproducibility

All quantitative data are presented as the mean ± s.d., as indicated for at least three independent experiments or biological replicates. Differences among groups were compared using a Student's *t*-test. *P* < 0.05 was considered statistically significant. Graphics and statistical analyses were carried out with Prism 6.0 (GraphPad Software) and Microsoft Excel v.15.19.1.
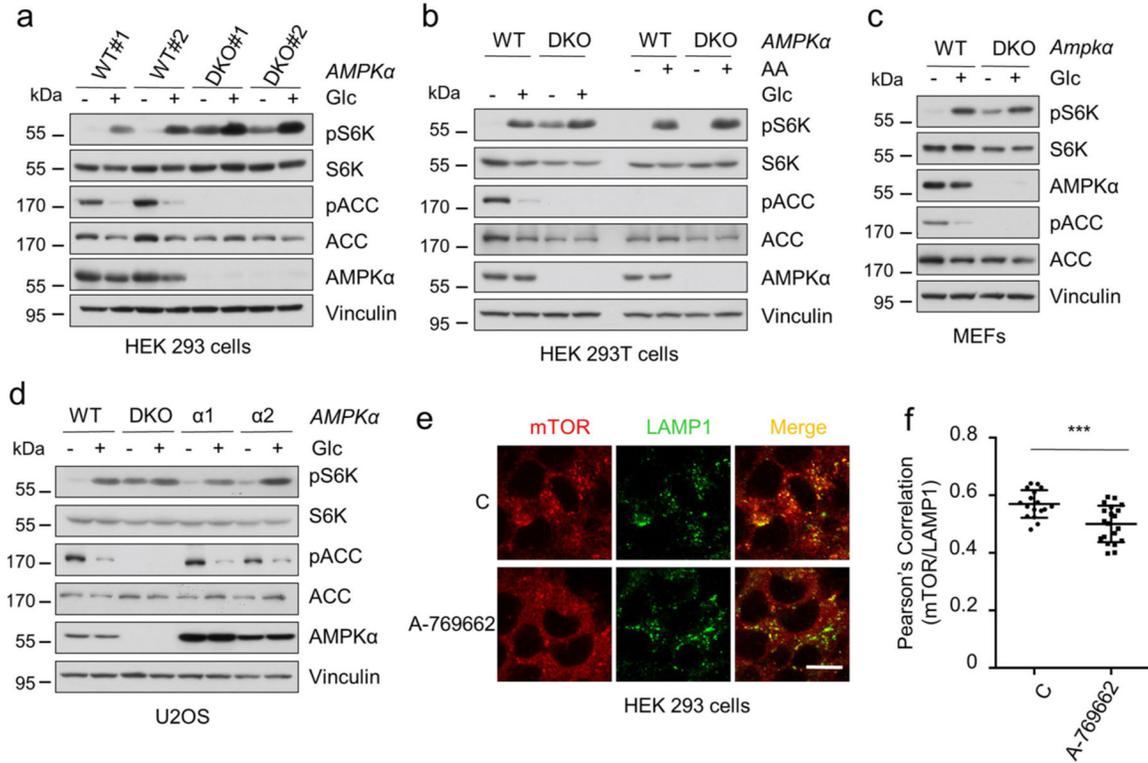
Extended Data
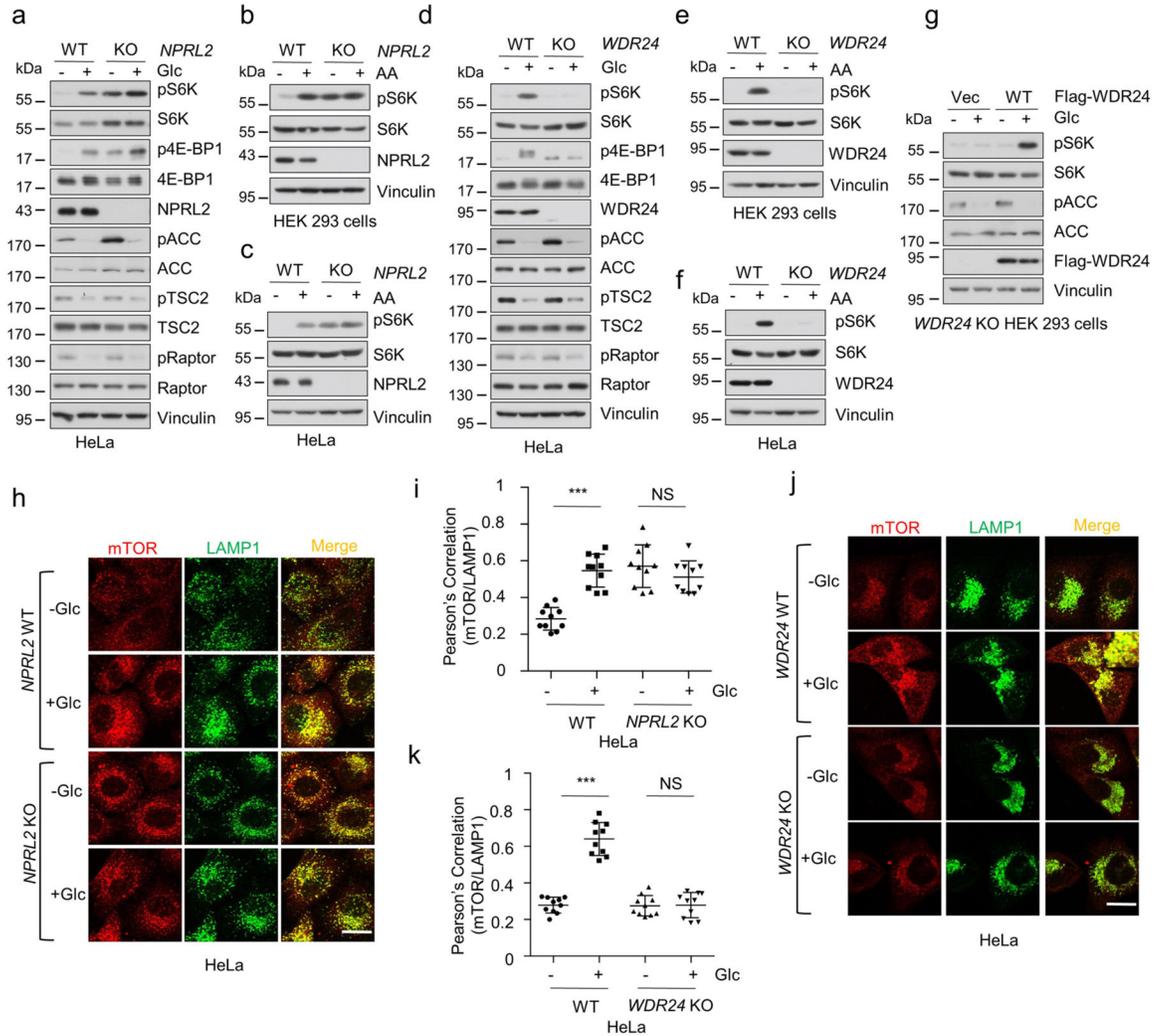
**Extended Data Fig. 1 |. GATOR1/2 complexes play an important role in mTORC1 glucose sensing.**

a, WT and *NPRL2* knockout (KO) HeLa cells were deprived of glucose (Glc) for 60 min and restimulated with glucose for 10 min as indicated. WCLs were analyzed via IB. **b,c**, WT and *NPRL2* KO HEK 293 (**b**) or HeLa (**c**) cells were deprived of amino acids (AA) for 60 min and restimulated with amino acids for 10 min as indicated. **d**, IB analysis of WCLs derived from WT and *WDR24* KO HeLa cells. The cells were treated as in (**a**). **e,f**, WT and *WDR24* KO HEK 293 (**e**) or HeLa (**f**) cells were deprived of amino acids for 60 min and restimulated with amino acids for 10 min as indicated. **g**, *WDR24* KO HEK 293 cells were re-introduced with or without WT WDR24, and the resulting cells were treated as in (**d**). **h,i**, WT and *NPRL2* KO HeLa cells were deprived of glucose for 60 min and restimulated with glucose for 10 min before coimmunostaining for mTOR (red) and LAMP1 (green) (**h**). Scale bar, 10 μm. The imaging data were quantified (**i**). n = 10. *P* = 4.93E-07, 0.21. Data are the mean ± s.d., two-tailed *t*-test. NS, not significant, ***P < 0.001. **j,k**, WT and *WDR24* KO HeLa cells were treated as in (**h,i**). The imaging data were quantified (**k**). Scale bar, 10 μm.

n = 10. *P* = 1.12E-09, 0.90. Data are the mean ± s.d., two-tailed *t*-test. NS, not significant, ***P < 0.001. Representative image shown, **a** and **d**, n = 3; **b**, **c**, **e**, **f** and **g**, n = 2.

**Extended Data Fig. 2 |. AMPK plays a pivotal role in mTORC1 glucose sensing.**
a, IB analysis of WCLs derived from WT and *AMPKα1/2* double knockout (DKO) HEK 293 cells. The cells were deprived of glucose for 60 min and restimulated with glucose for 10 min as indicated. **b**, IB analysis of WCLs derived from WT and *AMPKα1/2* DKO HEK 293 T cells. The cells were deprived of glucose or amino acids for 60 min and restimulated with glucose or amino acids for 10 min as indicated. **c**, IB analysis of WCLs derived from WT and *Ampkα1/2* DKO MEFs. The cells were treated as in (**a**). **d**, IB analysis of WCLs derived from WT, *AMPKα1/2* DKO, *AMPKα1* and *AMPKα2* reconstituted *AMPKα1/2* DKO U2OS cells. The cells were treated as in (**a**). **e**,**f**, HEK 293 cells were treated with or without A-769662 (100 μM) for 60 min, and the co-localization of mTORC1 (Red) and LAMP1 (green) was analyzed via immunofluorescence (**e**). Scale bar, 10 μm. The imaging data were quantified (**f**). n = 17, 20. *P* = 0.00058. Data are the mean ± s.d., two-tailed *t*-test. NS, not significant, ***P < 0.001. Representative image shown, **a**, **b** and **d**, n = 2; **c**, n = 3.
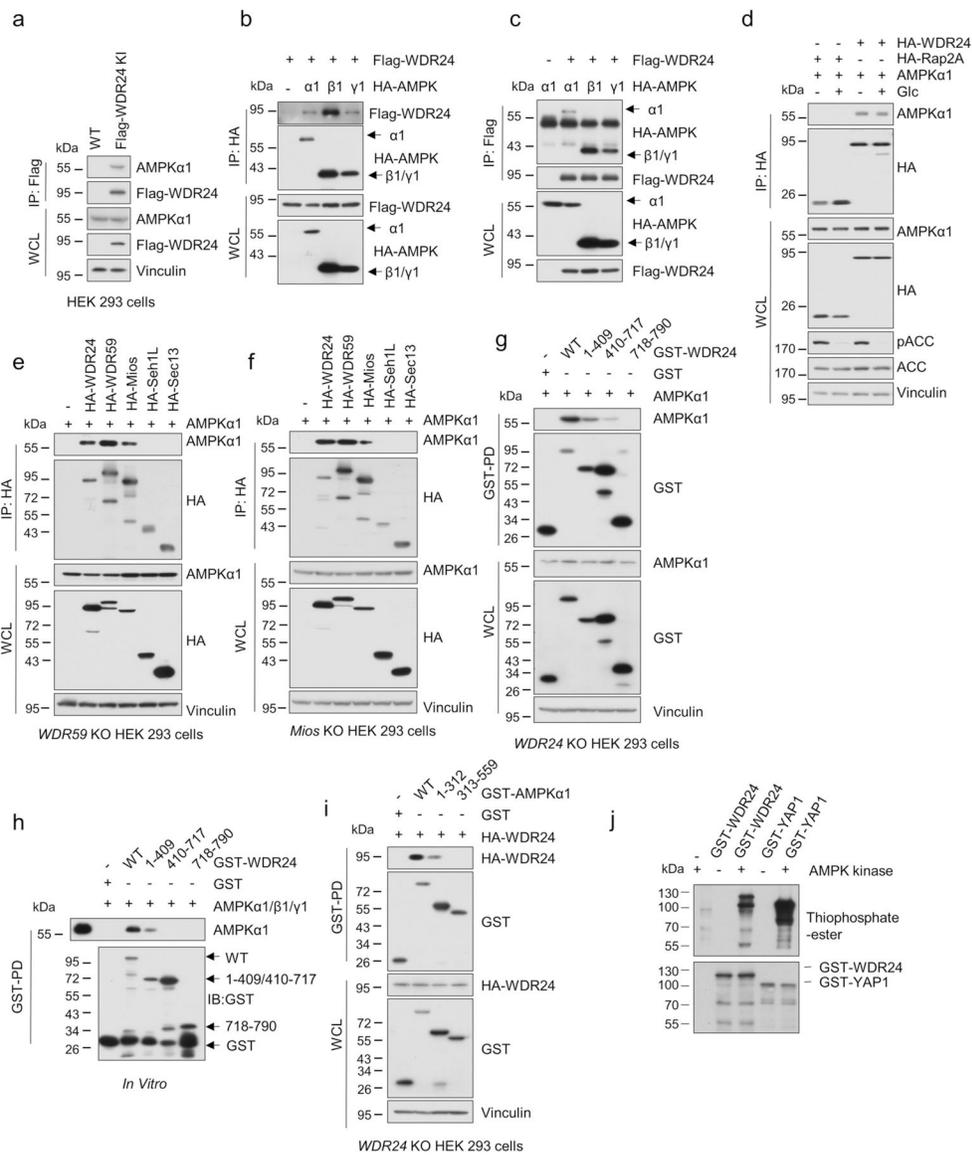
Extended Data Fig. 3 |. AMPK interacts with and phosphorylates WDR24.
a, IB analysis of WCLs and anti-Flag IPs derived from WT and *WDR24 Flag* knockin (KI) HEK 293 cells. **b,c**, IB analysis of WCLs and anti-HA or anti-Flag IPs derived from 293 T cells transfected with the indicated constructs. **d**, IB analysis of WCLs and anti-HA IPs derived from 293 T cells transfected with the indicated constructs. The cells were deprived of glucose for 60 min and restimulated with glucose for 10 min before harvesting. **e,f**, IB analysis of WCLs and anti-HA IPs derived from *WDR59* (**e**) or *Mios* (**f**) KO HEK 293 cells transfected with the indicated constructs. **g**, IB analysis of WCLs and GST-Pull down derived from *WDR24* KO HEK 293 cells transfected with the indicated constructs. **h**, Bacterial purified GST-WDR24 fragments were incubated with full-length human AMPK (combination of A1/B1/G2 subunits) which was expressed by baculovirus in Sf9 insect cells using a C-terminal His tag (SignalChem) for 3 h at 4 °C. **i**, IB analysis of WCLs and GST-Pull down derived from *WDR24* KO HEK 293 cells transfected

with the indicated constructs. **j**, *In vitro* kinase assay of indicated proteins demonstrates that AMPK phosphorylates WDR24. GST-WDR24 and YAP1 proteins were bacterially purified as substrates, and recombinant active AMPK was used as the source of kinase. Anti-thiophosphate-ester antibody was used to detect phosphorylated proteins. GST-YAP1 as a positive control. Representative image shown, **a**, n = 3; **b-j**, n = 2.
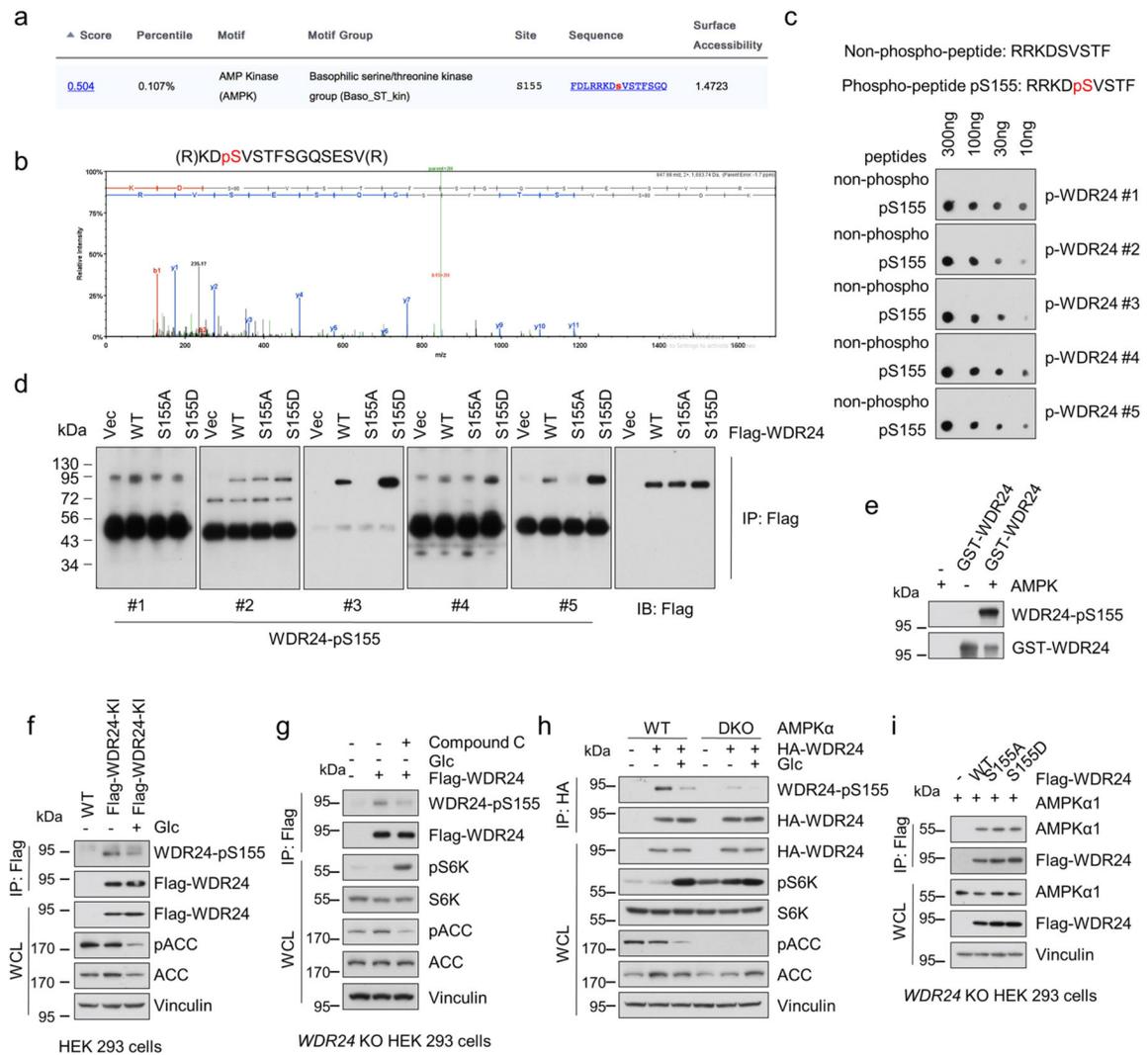
Extended Data Fig. 4 |. AMPK phosphorylates WDR24 on the S155 residue.
a, Scansite shows that WDR24 has a possible AMPK phosphorylation site. **b**, The MS/MS fragmentation spectrum showing fragment ions for the WDR24 peptide KDpSVSTFSGQSESV defining the WDR24-pS155 site. **c**, Titration of the indicated WDR24 peptides with or without S155 phosphorylation demonstrates that the generated WDR24-pS155 antibodies specifically recognize the pS155 epitope in the dot blot analysis. **d**, IB analysis of anti-Flag IPs derived from 293 T cells transfected with indicated constructs to demonstrate that mutating the Ser155 site in WDR24 abolished the ability of the generated WDR24-pS155 antibody (#3 and #5) to recognize WDR24 phosphorylated species in cells. **e**, *In vitro* kinase assays demonstrated that the WDR24-pS155 antibody

recognizes the phosphorylated WDR24. GST-WDR24 protein was purified from *E. coli*, and recombinant active AMPK was used as the source of kinase. **f**, IB analysis of WCLs and anti-Flag IPs derived from WT and *WDR24 Flag* knock-in HEK 293 cells. The cells were deprived of glucose for 60 min and restimulated with glucose for 10 min as indicated. **g**, *WDR24* KO HEK 293 cells reconstituted with WT-WDR24 were starved of glucose and treated with Compound C (10 μM) for 1 h before harvesting for IB analysis. **h**, IB analysis of WCLs and anti-HA IPs derived from WT or *AMPKα1/2* DKO HEK 293 T cells transfected with indicated constructs. The cells were deprived of glucose for 60 min and restimulated with glucose for 10 min as indicated. **i**, IB analysis of WCLs and anti-Flag IPs derived from *WDR24* KO HEK 293 cells reconstituted with indicated constructs. Representative image shown, **e**-**i**, n = 2.
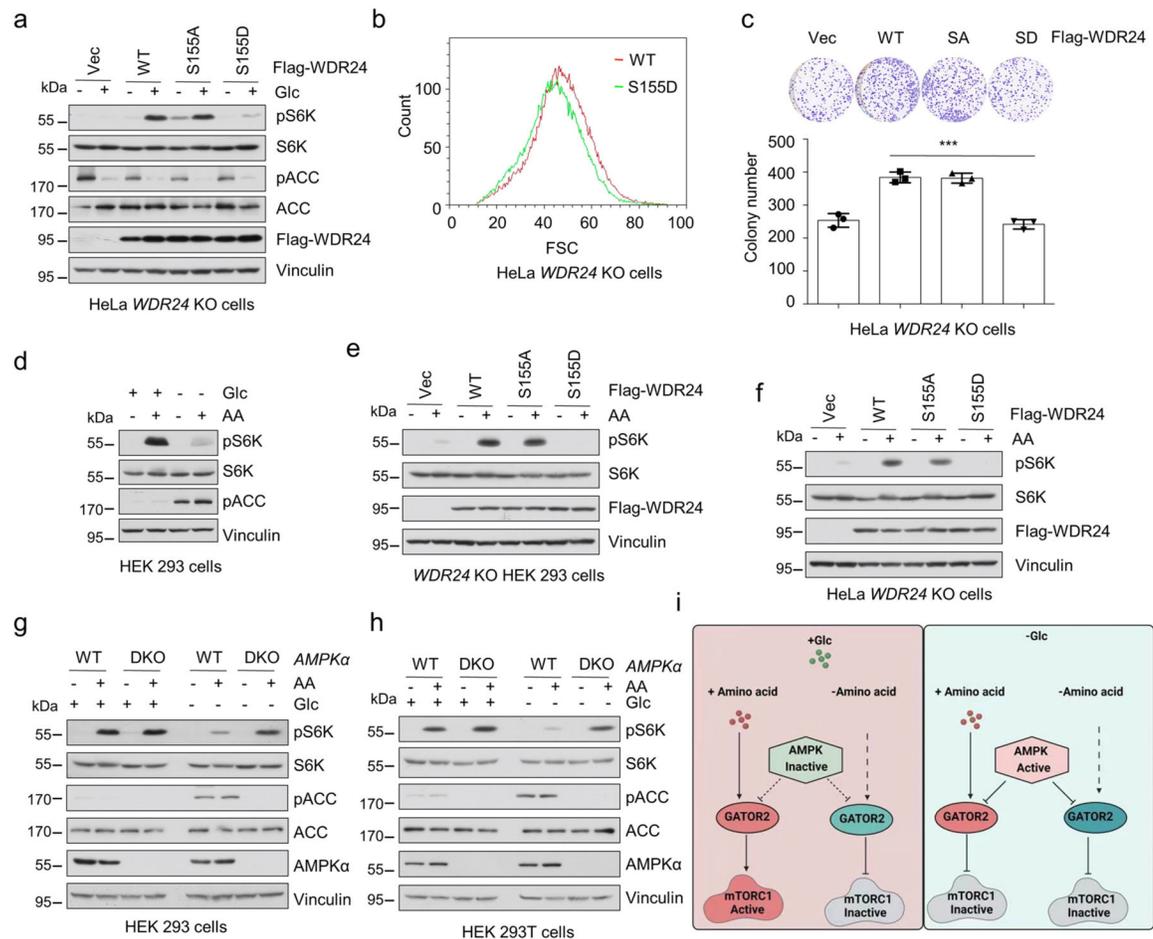
Extended Data Fig. 5 |. Phosphorylation of S155 on WDR24 inhibits the activation of mTORC1 induced by glucose.
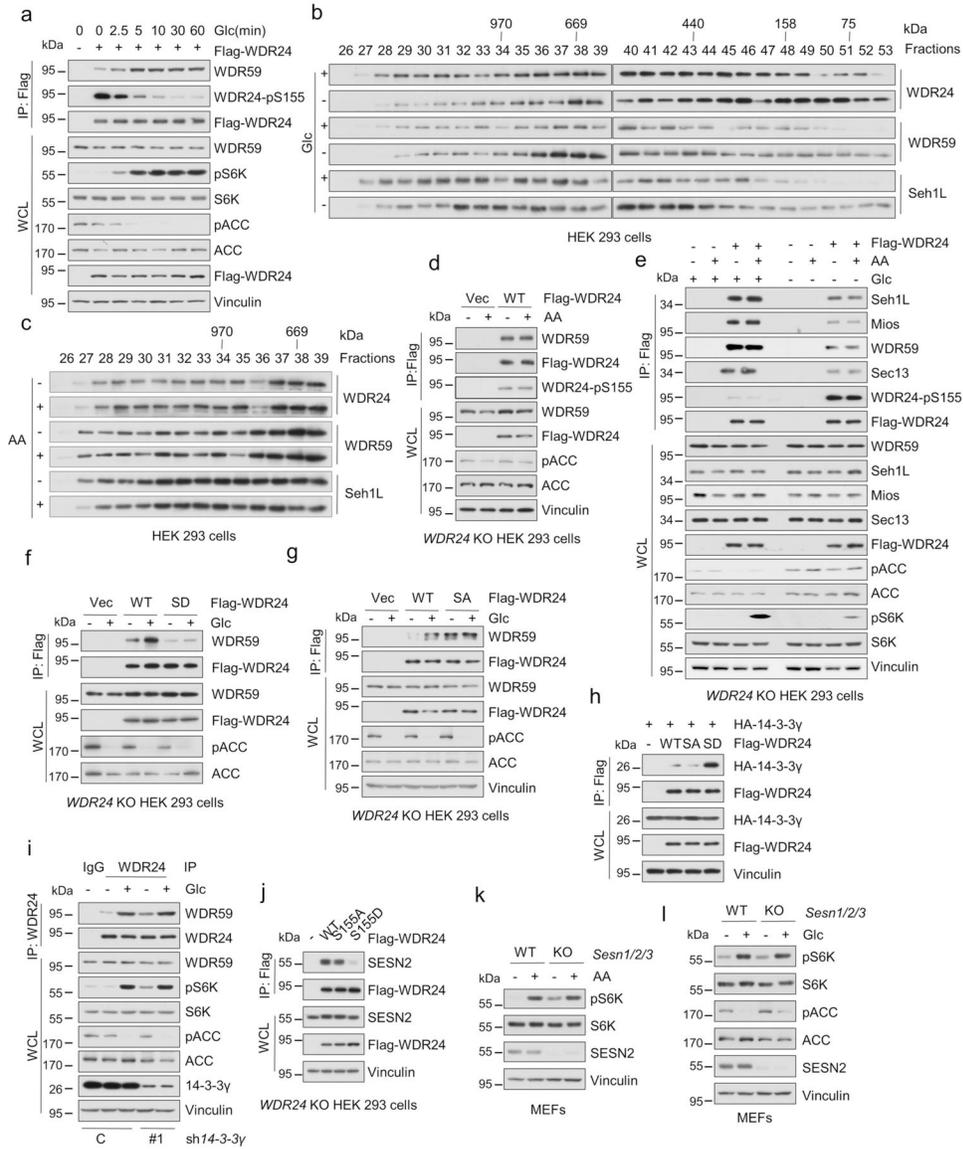
a, *WDR24* KO HeLa cells reintroduced with indicated constructs were deprived of glucose for 60 min and restimulated with glucose for 10 min as indicated. **b**, Cell size histogram of *WDR24* KO HeLa cells reconstituted with WT and WDR24 S155D by FACS. **c**, *WDR24* KO HeLa cells reconstituted with indicated constructs were plated for 8 d for the colony-formation assays. Data are shown as the mean ± s.d. of n = 3 independent experiments

(bottom). $P = 0.0004$. two-tailed t-test. ***$P < 0.001$. **d**, IB analysis of WCLs of HEK 293 cells starved of glucose or/and amino acids for 1 h, and restimulated with amino acids for 10 min. **e**, *WDR24* KO HEK 293 cells re-introduced with indicated constructs were deprived of amino acids for 60 min and restimulated with amino acids for 10 min as indicated before IB analysis. **f**, *WDR24* KO HeLa cells were re-introduced with indicated constructs. The cells were treated as in (**e**). **g,h**, WT and *AMPKα1/2* DKO HEK 293 (**g**) or 293 T (**h**) cells were starved of amino acids or amino acids and glucose together for 60 min, then stimulated with amino acids for 10 min. **i**, Working model to show how AMPK regulates mTORC1 amino acid sensing under energy stress conditions. Representative image shown, **a** and **d**, n = 3; **e**, **f**, **g** and **h**, n = 2.
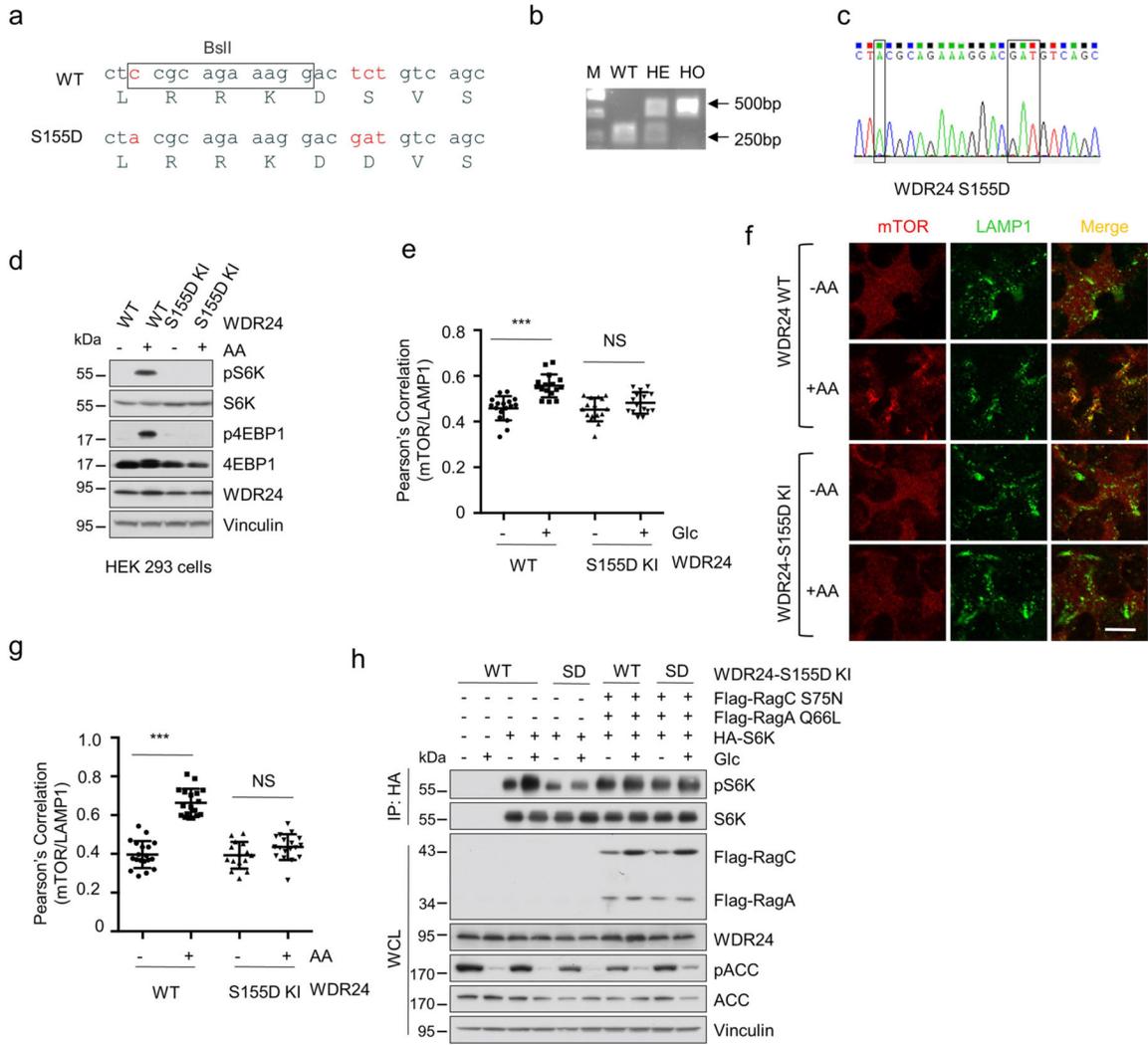
Extended Data Fig. 6 |. The WDR24-S155D mutation inhibits mTORC1 kinase activity.
a, Schematic representation of the amino sequence to generate *WDR24-S155D* CRISPR knock-in cells. **b**, Identification of the potential knock-in mutants. Genomic DNA containing *WDR24-S155D* mutation was amplified by PCR and digested with BslI. **c**, Confirmation of the correct mutation of Raptor-S606D or S606A by Sanger DNA sequencing. **d**, WT

and *WDR24-S155D* knock-in 293 cells were deprived of amino acids for 60 min and restimulated with amino acids for 10 min as indicated. Representative image shown, n = 3. **e**, WT and *WDR24-S155D* knock-in 293 cells were deprived of glucose for 60 min and restimulated with glucose for 10 min before immunostaining for mTOR and LAMP1. The imaging data were quantified under each condition. n = 17, 16, 16, 15. P = 5.67E-06, 0.11. Data are the mean ± s.d., two-tailed *t*-test. NS, not significant, ***P < 0.001. See Fig. 4e for imaging data. **f,g**, WT and *WDR24-S155D* knock-in 293 cells were deprived of amino acids for 60 min and restimulated with amino acids for 10 min before coimmunostaining for mTOR (red) and LAMP1 (green) (**f**). Scale bar, 10 μm. The imaging data were quantified with 10–20 cells under each condition (**g**). n = 19, 18, 15, 18. P = 2.56E-13, 0.08. Data are the mean ± s.d., two-tailed *t*-test. NS, not significant. ***P < 0.001. **h**, IB analysis of WCLs and anti-HA IPs derived from WT and *WDR24-S155D* knock-in HEK 293 cells transfected with the indicated constructs. The cells were deprived of glucose for 60 min and restimulated with glucose for 10 min before harvesting. Representative image shown, n = 2.

Extended Data Fig. 7 |. Glucose deprivation regulates GATOR2 complex integrity through phosphorylating WDR24 on S155.

a, IB analysis of WCLs and anti-Flag IPs derived from *WDR24* KO HEK 293 cells reconstituted with indicated constructs. The cells were deprived of glucose for 60 min and restimulated with glucose for different time points as indicated. **b**, WCLs of HEK 293 cells deprived of glucose for 60 min and restimulated with glucose for 10 min as indicated were run through a Superose 6 Increase 10/300 GL column. Elutes were collected for each fraction and analyzed by IB analysis. **c**, WCLs of HEK 293 cells were deprived of amino acids for 60 min and restimulated with amino acids for 10 min as indicated and analyzed as (**b**). **d**, IB analysis of WCLs and anti-Flag IPs derived from *WDR24* KO HEK 293 cells reconstituted with indicated constructs. The cells were deprived of amino acids for 60 min and restimulated with amino acids for 10 min as indicated. **e**, IB analysis of WCLs and anti-Flag IPs derived from *WDR24* KO HEK 293 cells reconstituted with indicated constructs. Cells were starved with amino acids or amino acids and glucose together for 60

min, then stimulated with amino acids for 10 min. **f,g**, IB analysis of WCLs and anti-Flag IPs derived from *WDR24* KO HEK 293 cells reconstituted with indicated constructs. The cells were deprived of glucose for 60 min and restimulated with glucose for 10 min as indicated. **h**, IB analysis of WCLs and IPs derived from HEK 293 cells transfected with indicated plasmids. **i**, IB analysis of WCLs and anti-WDR24 IPs derived from WT and *14-3-3γ* knockdown HEK 293 cells. The cells were treated as (**f,g**). **j**, IB analysis of WCLs and anti-Flag IPs derived from *WDR24* KO HEK 293 cells reconstituted with indicated constructs. **k,l**, Wild-type (WT) and *Sesn1/2/3* knockout MEFs were deprived of amino acids (AA) (**k**) or glucose (Glc) (**l**) for 60 min and restimulated with amino acids for 10 min as indicated. WCLs were analyzed via IB. Representative image shown, **a-j** and **i**, n = 2; **k**, n = 3.
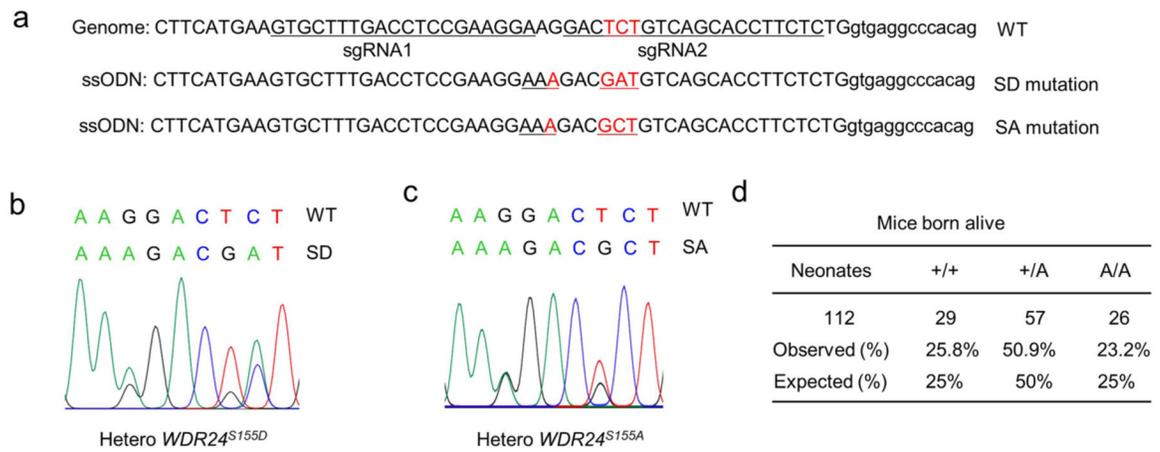
Extended Data Fig. 8 |. Generation of *Wdr24S155D* and *Wdr24S155A* knock-in mice by CRISPR-Cas9-mediated genome editing.

a, sgRNA sequence and part of ssODN sequence used for generating *Wdr24^S155A/D^* knock-in mice. **b**, Sanger sequencing results of hetero *Wdr24^S155D^* knock-in mouse genomic DNA. **c**, Sanger sequencing results of hetero *Wdr24^S155A^* knock-in mouse genomic DNA. **d**, Neonates from *WDR24^+/A^* parents were counted at birth.
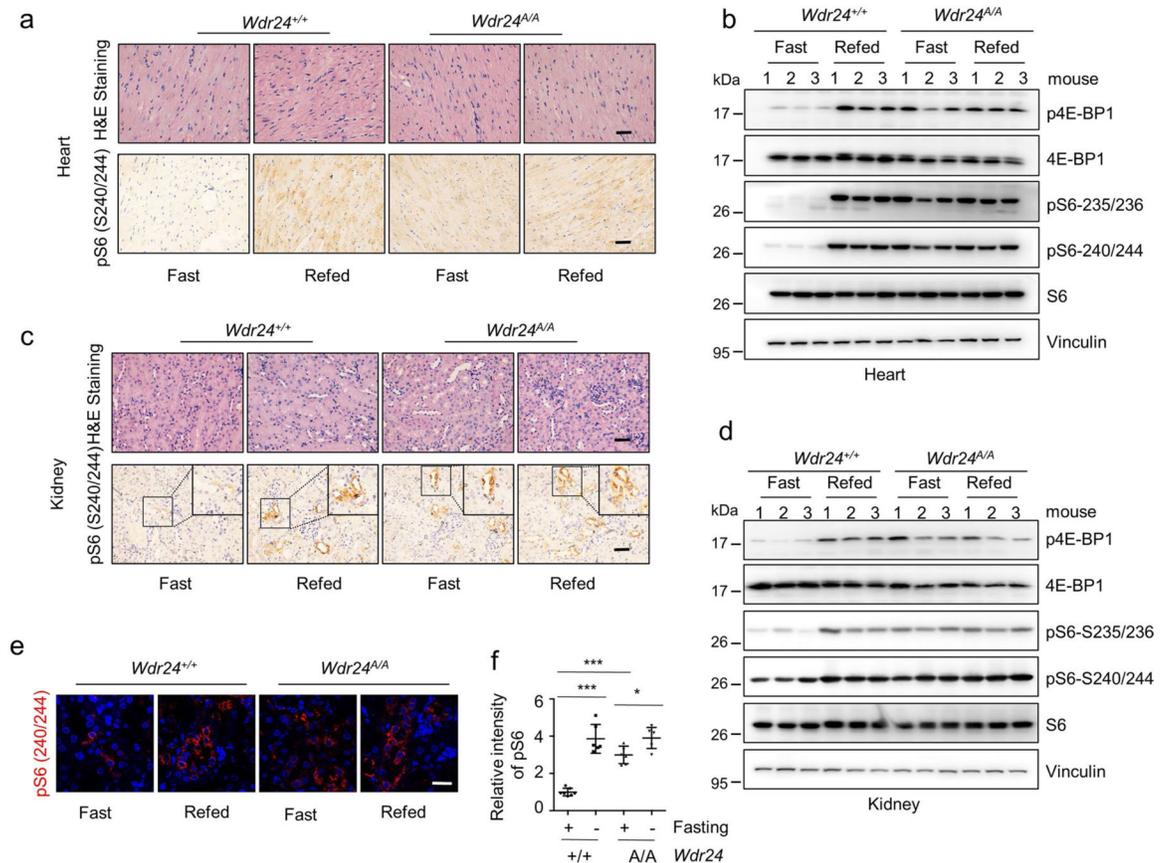
Extended Data Fig. 9 |. Phospho-deficient *Wdr24S155A* knock-in mice show relatively high mTORC1 activity under fasting.

a, Representative images of hematoxylin and eosin (H&E) (scale bar, 50 μm), p-S6(S40/244) (scale bar, 100 μm) staining of the heart section (n = 3) of *Wdr24+/+*and *Wdr24A/A* littermates. The mice were fasted for 24 h, or fasted and refed for 2 h. **b**, IB analysis of WCLs derived from *Wdr24+/+*or *Wdr24A/A* mouse livers. The mice were fasted for 24 h, or fasted and refed for 2 h. n = 3 mice. **c**, Representative images of hematoxylin and eosin (H&E) (scale bar, 50 μm), p-S6(S240/244) staining (scale bar, 100 μm; insets magnification=1.5) of the kidney section (n = 3) of *Wdr24+/+*and *Wdr24A/A* littermates. The mice were fasted for 24 h, or fasted and refed for 2 h. **d**, IB analysis of WCLs derived from *Wdr24+/+*or *Wdr24A/A* mouse kidneys. The mice were fasted for 24 h or fasted and refed for 2 h. n = 3 mice. **e**,**f**, IF analysis of the kidney section of *Wdr24+/+*and *Wdr24A/A* littermates (**e**). Scale bar, 20 μm. The mice were fasted for 24 h, or fasted and refed for 2 h. The pS6 (240/244) intensity was quantified via Image J (**f**). n = 7, 6, 6, 6. *P*= 1.27E-06, 5.95E-07, 0.01. Data are mean ± s.d., two-tailed *t*-test. **P*< 0.05, ****P*< 0.001.
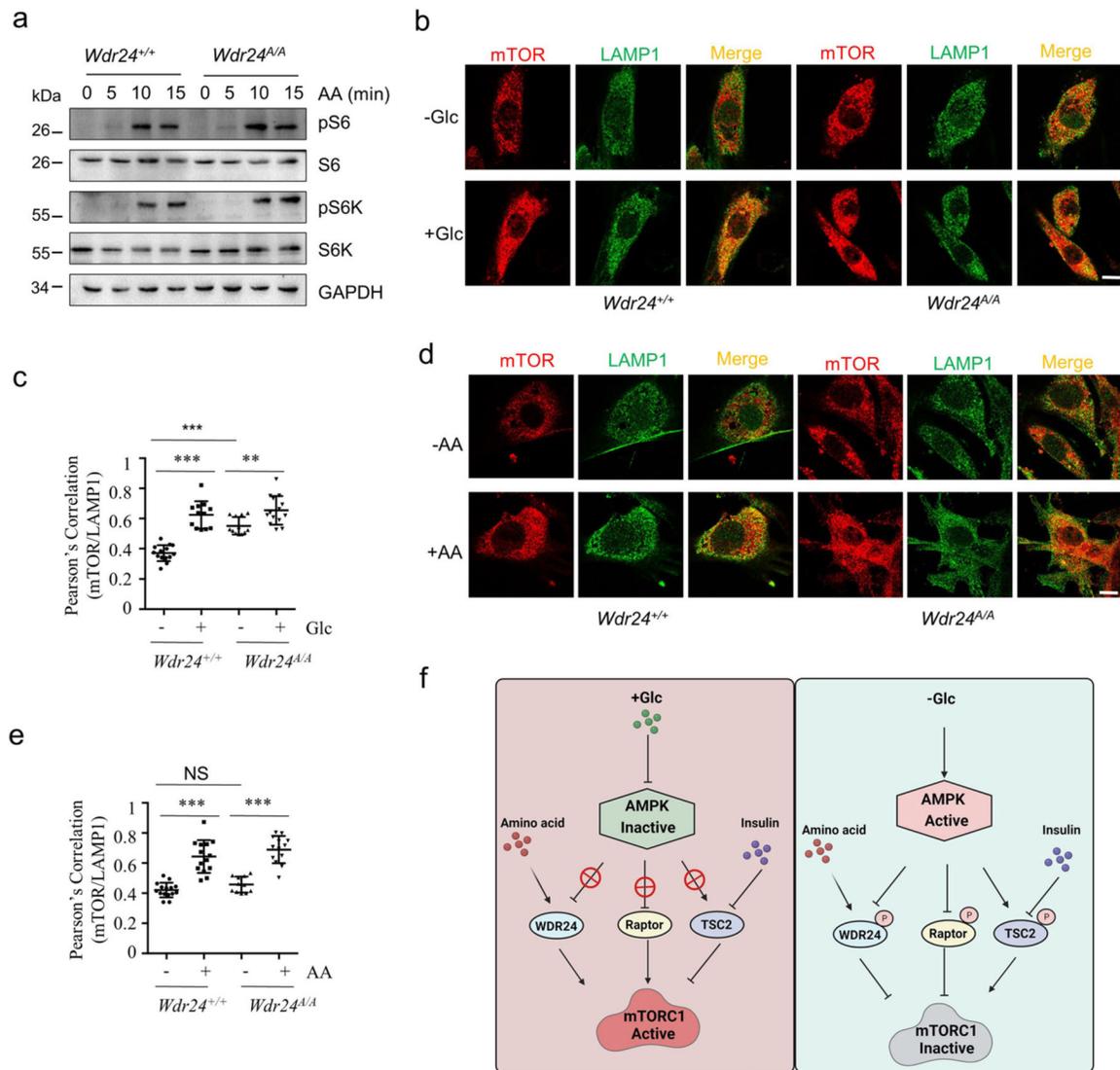
Extended Data Fig. 10 |. The WDR24-S155A mutation partially regulates mTORC1 lysosome localization under glucose starvation.

a, IB analysis of WCLs derived from *Wdr24*^{+/+} or *Wdr24*[A/A] MEFs. The cells were deprived of amino acids for 60 min and restimulated with amino acids for 10 min as indicated. Representative image shown, n = 2. **b**, IF analysis of *Wdr24*^{+/+} or *Wdr24*[A/A] MEFs. Indicated cells were deprived of glucose for 60 min and restimulated with glucose for 10 min as indicated. Scale bar, 10 μm. **c**, The imaging data in (**b**) were quantified. n = 14, 12, 12, 14. $P = 4.74E-09$, $1.57E-08$, 0.003. Data are the mean ± s.d., two-tailed *t*-test. ***$P < 0.01$, ***$P < 0.001$. **d**, IF analysis of *Wdr24*^{+/+} or *Wdr24*[A/A] MEFs. Indicated cells were deprived of amino acids for 60 min and restimulated with amino acids for 10 min as indicated. Scale bar, 10 μm. **e**, The imaging data in (**d**) were quantified. n = 15, 14, 11, 13. $P = 1.05E-07$, 0.08, $1.72E-07$. Data are the mean ± s.d., two-tailed *t*-test. NS, not significant. ***$P < 0.001$. **f**, A working model to show how glucose regulates mTORC1 kinase activity through AMPK-mediated WDR24, Raptor and TSC2 phosphorylation.

Supplementary Material

Refer to Web version on PubMed Central for supplementary material.

Data availability

All data that support the findings of this study are available in the figures or Extended Data figures. Mass spectrometry fragmentation spectra were searched against the concatenated decoy human protein database v.20210315 (UniProt). Source data are provided with this paper.

References

1. DeBerardinis RJ, Lum JJ, Hatzivassiliou G & Thompson CB The biology of cancer: metabolic reprogramming fuels cell growth and proliferation. Cell Metab 7, 11–20 (2008). [PubMed: 18177721]

2. Vander Heiden MG, Cantley LC & Thompson CB Understanding the Warburg effect: the metabolic requirements of cell proliferation. Science 324, 1029–1033 (2009). [PubMed: 19460998]

3. Rabinowitz JD & White E Autophagy and metabolism. Science 330, 1344–1348 (2010). [PubMed: 21127245]

4. Saxton RA & Sabatini DM mTOR signaling in growth, metabolism, and disease. Cell 168, 960–976 (2017). [PubMed: 28283069]

5. Kim J & Guan KL mTOR as a central hub of nutrient signalling and cell growth. Nat. Cell Biol 21, 63–71 (2019). [PubMed: 30602761]

6. Bar-Peled L et al. A tumor suppressor complex with GAP activity for the Rag GTPases that signal amino acid sufficiency to mTORC1. Science 340, 1100–1106 (2013). [PubMed: 23723238]

7. Wolfson RL & Sabatini DM The dawn of the age of amino acid sensors for the mTORC1 pathway. Cell Metab 26, 301–309 (2017). [PubMed: 28768171]

8. Wolfson RL et al. Sestrin2 is a leucine sensor for the mTORC1 pathway. Science 351, 43–48 (2016). [PubMed: 26449471]

9. Chantranupong L et al. The CASTOR proteins are arginine sensors for the mTORC1 pathway. Cell 165, 153–164 (2016). [PubMed: 26972053]

10. Chen J et al. SAR1B senses leucine levels to regulate mTORC1 signalling. Nature 596, 281–284 (2021). [PubMed: 34290409]

11. Orozco JM et al. Dihydroxyacetone phosphate signals glucose availability to mTORC1. Nat. Metab 2, 893–901 (2020). [PubMed: 32719541]

12. Hardie DG, Ross FA & Hawley SA AMPK: a nutrient and energy sensor that maintains energy homeostasis. Nat. Rev. Mol. Cell Biol 13, 251–262 (2012). [PubMed: 22436748]

13. Herzig S & Shaw RJ AMPK: guardian of metabolism and mitochondrial homeostasis. Nat. Rev. Mol. Cell Biol 19, 121–135 (2018). [PubMed: 28974774]

14. Lin S-C & Hardie DG AMPK: sensing glucose as well as cellular energy status. Cell Metab 27, 299–313 (2018). [PubMed: 29153408]

15. Inoki K, Zhu T & Guan K-L TSC2 mediates cellular energy response to control cell growth and survival. Cell 115, 577–590 (2003). [PubMed: 14651849]

Author Manuscript Author Manuscript Author Manuscript Author Manuscript

16. Van Nostrand JL et al. AMPK regulation of Raptor and TSC2 mediate metformin effects on transcriptional control of anabolism and inflammation. Genes Dev 34, 1330–1344 (2020). [PubMed: 32912901]

17. Gwinn DM et al. AMPK phosphorylation of raptor mediates a metabolic checkpoint. Mol. Cell 30, 214–226 (2008). [PubMed: 18439900]

18. Efeyan A et al. Regulation of mTORC1 by the Rag GTPases is necessary for neonatal autophagy and survival. Nature 493, 679–683 (2013). [PubMed: 23263183]

19. Wolfson RL et al. KICSTOR recruits GATOR1 to the lysosome and is necessary for nutrients to regulate mTORC1. Nature 543, 438–442 (2017). [PubMed: 28199306]

20. Sancak Y et al. Ragulator-Rag complex targets mTORC1 to the lysosomal surface and is necessary for its activation by amino acids. Cell 141, 290–303 (2010). [PubMed: 20381137]

21. Shaw RJ et al. The LKB1 tumor suppressor negatively regulates mTOR signaling. Cancer Cell 6, 91–99 (2004). [PubMed: 15261145]

22. Cool B et al. Identification and characterization of a small molecule AMPK activator that treats key components of type 2 diabetes and the metabolic syndrome. Cell Metab 3, 403–416 (2006). [PubMed: 16753576]

23. Shen K et al. Architecture of the human GATOR1 and GATOR1–Rag GTPases complexes. Nature 556, 64–69 (2018). [PubMed: 29590090]

24. Hardie DG, Schaffer BE & Brunet A AMPK: an energy-sensing pathway with multiple inputs and outputs. Trends Cell Biol 26, 190–201 (2016). [PubMed: 26616193]

25. Zhou G et al. Role of AMP-activated protein kinase in mechanism of metformin action. J. Clin. Invest 108, 1167–1174 (2001). [PubMed: 11602624]

26. Xiao B et al. Structural basis of AMPK regulation by small molecule activators. Nat. Commun 4, 3017 (2013). [PubMed: 24352254]

27. Liu GY & Sabatini DM mTOR at the nexus of nutrition, growth, ageing and disease. Nat. Rev. Mol. Cell Biol 21, 183–203 (2020). [PubMed: 31937935]

28. Peng M, Yin N & Li MO SZT2 dictates GATOR control of mTORC1 signalling. Nature 543, 433–437 (2017). [PubMed: 28199315]

29. Bridges D & Moorhead GBG 14-3-3 proteins: a number of functions for a numbered protein. Sci. STKE 2005, re10 (2005).

30. Valenstein ML et al. Structure of the nutrient-sensing hub GATOR2. Nature 607, 610–616 (2022). [PubMed: 35831510]

31. Efeyan A et al. RagA, but not RagB, is essential for embryonic development and adult mice. Dev. Cell 29, 321–329 (2014). [PubMed: 24768164]

32. Gonzalez A, Hall MN, Lin S-C & Hardie DG AMPK and TOR: the Yin and Yang of cellular nutrient sensing and growth control. Cell Metab 31, 472–492 (2020). [PubMed: 32130880]

33. Leprivier G & Rotblat B How does mTOR sense glucose starvation? AMPK is the usual suspect. Cell Death Discov 6, 27 (2020). [PubMed: 32351714]

34. Lee MN et al. Glycolytic flux signals to mTOR through glyceraldehyde-3-phosphate dehydrogenase-mediated regulation of Rheb. Mol. Cell. Biol 29, 3991–4001 (2009). [PubMed: 19451232]

35. Roberts DJ, Tan-Sah VP, Ding EY, Smith JM & Miyamoto S Hexokinase-II positively regulates glucose starvation-induced autophagy through TORC1 inhibition. Mol. Cell 53, 521–533 (2014). [PubMed: 24462113]

36. Zhang CS et al. Fructose-1,6-bisphosphate and aldolase mediate glucose sensing by AMPK. Nature 548, 112–116 (2017). [PubMed: 28723898]

37. Almacellas E et al. Phosphofructokinases axis controls glucose-dependent mTORC1 activation driven by E2F1. iScience 20, 434–448 (2019). [PubMed: 31627130]

38. Gan W et al. LATS suppresses mTORC1 activity to directly coordinate Hippo and mTORC1 pathways in growth control. Nat. Cell Biol 22, 246–256 (2020). [PubMed: 32015438]

39. Dai X et al. Energy status dictates PD-L1 protein abundance and anti-tumor immunity to enable checkpoint blockade. Mol. Cell 81, 2317–2331 (2021). [PubMed: 33909988]

40. Liu P et al. Sin1 phosphorylation impairs mTORC2 complex integrity and inhibits downstream Akt signalling to suppress tumorigenesis. Nat. Cell Biol 15, 1340–1350 (2013). [PubMed: 24161930]
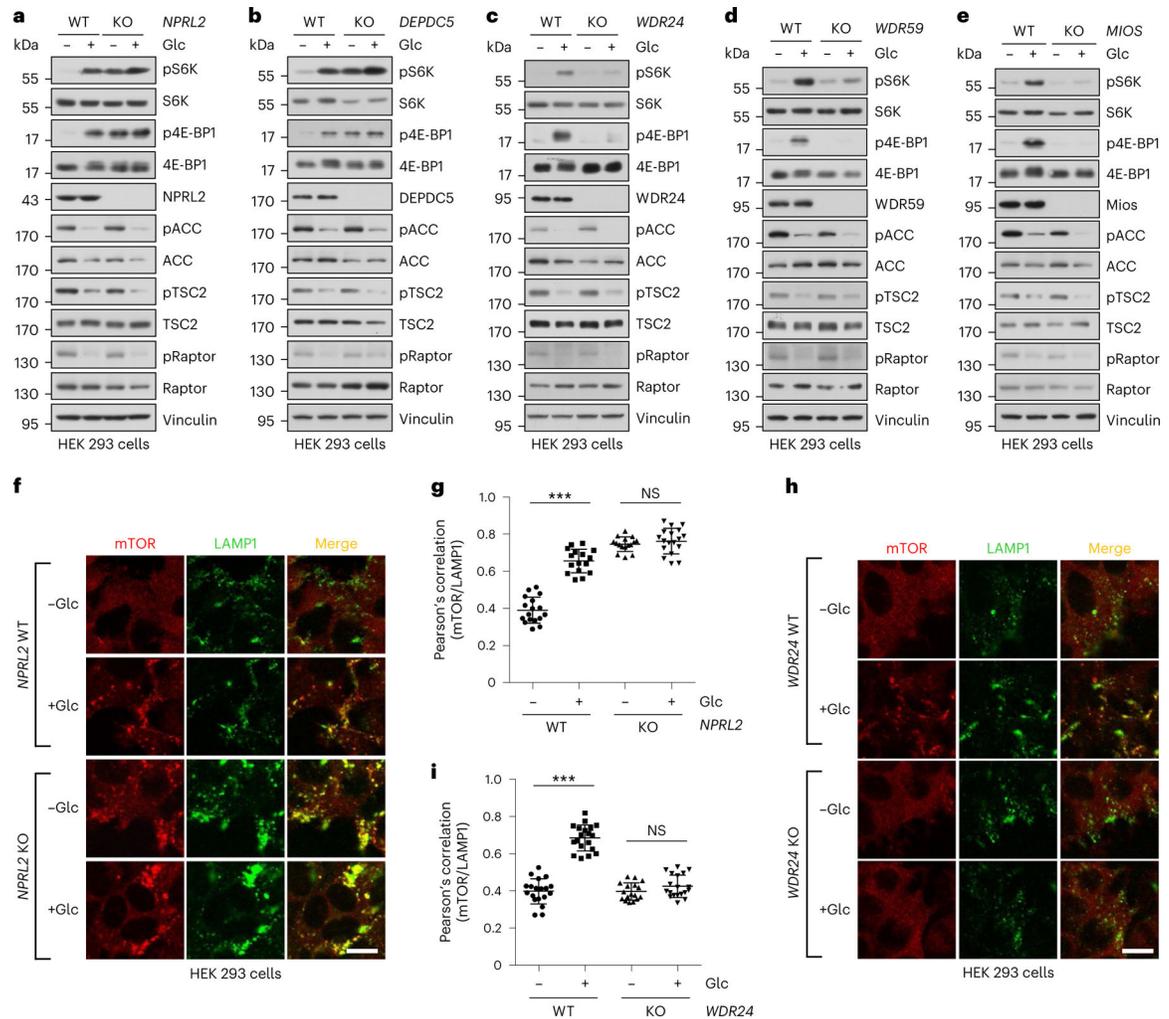
Fig. 1 |. The GATOR1/2 complexes regulate mTORC1 glucose sensing.
a–e, WT and *NPRL2* (**a**)*, DEPDC5* (**b**), *WDR24* (**c**), *WDR59* (**d**) and *MIOS* (**e**) knockout (KO) HEK 293 cells were deprived of glucose (Glc) for 60 min and restimulated with Glc for 10 min as indicated. WCLs were analysed via IB by probing with the indicated antibodies. Representative image shown. In **a–e**, $n = 3$. **f,g**, WT and *NPRL2* knockout HEK 293 cells were treated as in **a–e** and the colocalization of mTORC1 (red) and LAMP1 (green) was analysed via immunostaining (**f**). Scale bar, 10 μm. The imaging data were quantified under each condition, $n = 17, 16, 16, 18$ (left to right) (**g**). $P = 1.25 \times 10^{-12}$, $P = 0.39$ (left to right). Data are the mean ± s.d., two-tailed *t*-test. NS, not significant, ***$P < 0.001$. **h,i**, WT and *WDR24* knockout HEK 293 cells were treated and analysed as in **f,g**. Scale bar, 10 μm. $n = 19, 19, 17, 19$. $P = 5.50 \times 10^{-15}$, $P = 0.12$. Data are the mean ± s.d., two-tailed *t*-test. ***$P < 0.001$.
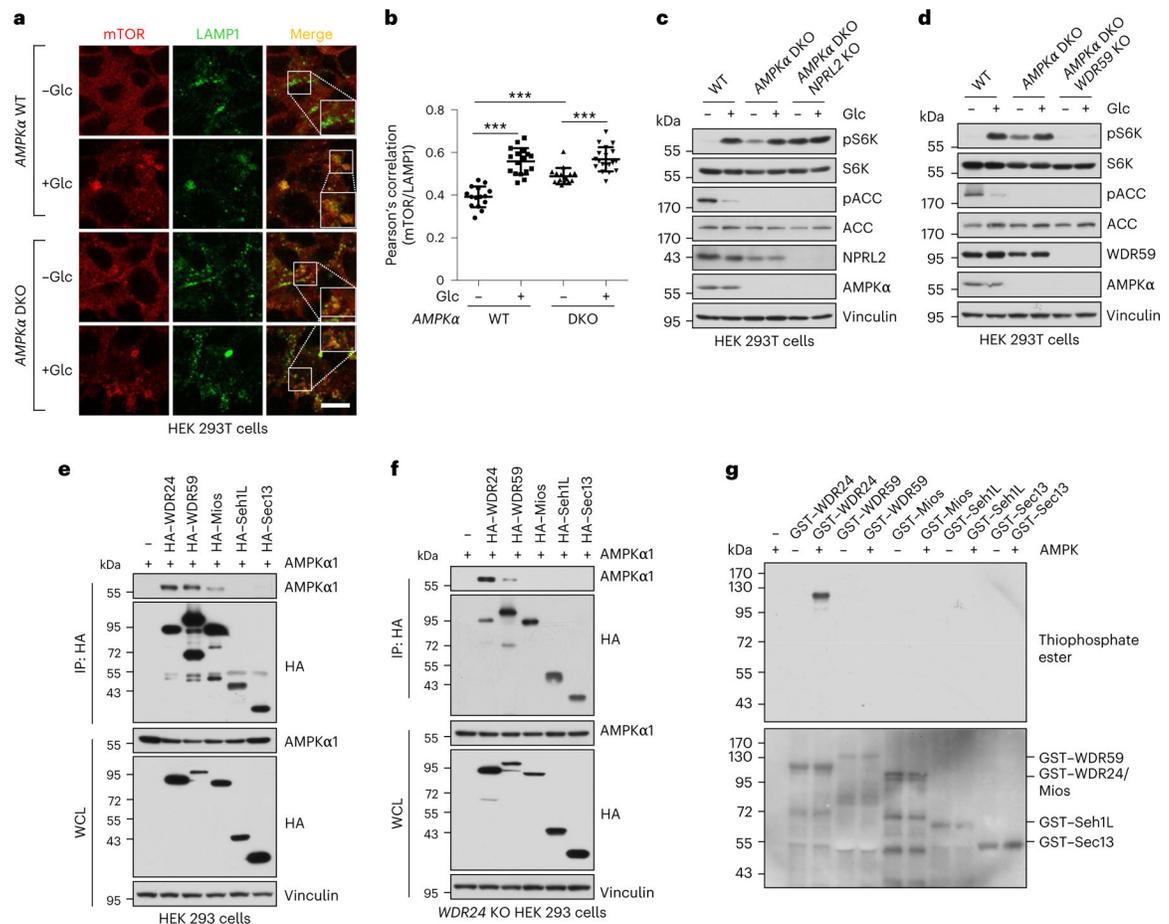
Fig. 2 |. The AMPK–GATOR1/2 axis regulates mTORC1 glucose sensing.
a,b, WT and *AMPKα1/α2* double knockout (DKO) HEK 293T cells were deprived of Glc for 60 min and restimulated with Glc for 10 min before immunostaining for mTOR (red) and LAMP1 (green) (**a**). Scale bar, 10 μm; insets magnification=1.5. The imaging data were quantified (**b**). $n = 15, 17, 16, 19$. $P = 2.24 \times 10^{-9}$, $P = 1.14 \times 10^{-6}$, $P = 4.25 \times 10^{-5}$. Data are the mean ± s.d.; two-tailed *t*-test. ****P* < 0.001. **c**, WT, *AMPKα1/α2* DKO and *AMPKα1/α2/NPRL2* triple-knockout HEK 293T cells were deprived of Glc for 60 min and restimulated with Glc for 10 min. WCLs were analysed via IB. **d**, WT, *AMPKα1/α2* DKO and *AMPKα1/α2/WDR59* triple-knockout HEK 293T cells were treated as in **c**. **e,f**, IB analysis of WCLs and anti-HA immunoprecipitates derived from WT (**e**) or *WDR24* KO (**f**) HEK 293 cells transfected with the indicated constructs. **g**, In vitro kinase assays of the indicated proteins demonstrate that AMPK phosphorylates WDR24. The GST–GATOR2 components were bacterially purified as substrates and recombinant active AMPK was used as the source of kinase. Anti-thiophosphate ester antibody was used to detect phosphorylated proteins. Representative image shown. In **c,d**, $n = 3$. In **e–g**, $n = 2$.
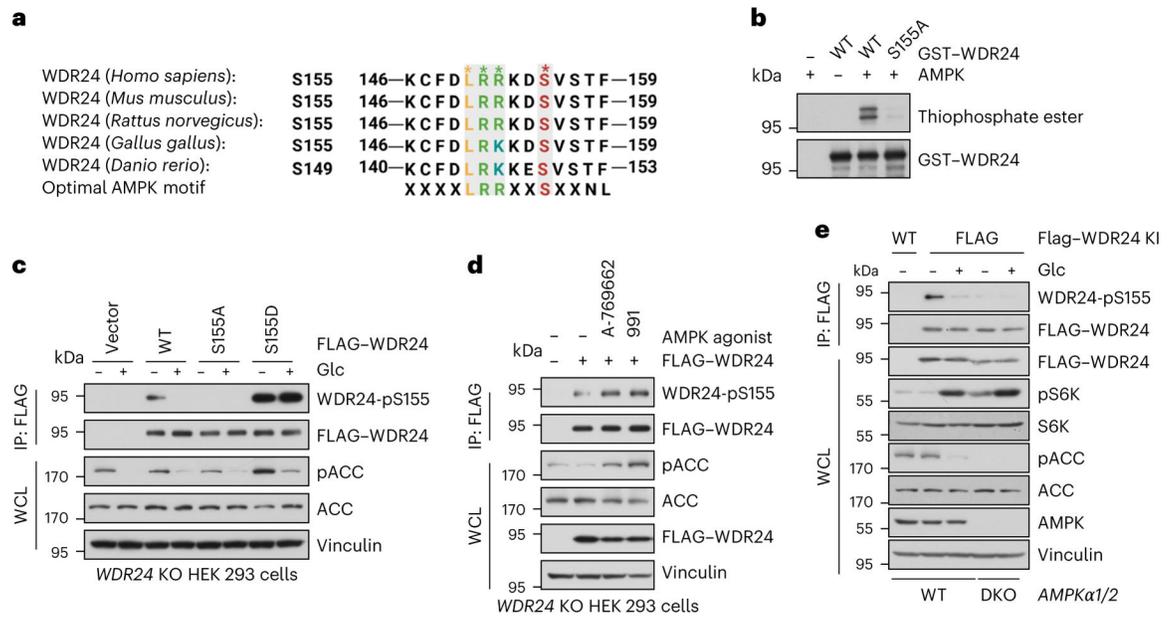
Fig. 3 |. AMPK phosphorylation of WDR24 on S155 is regulated by glucose availability.
a, Schematic presentation of the evolutionarily conserved putative AMPK phosphorylation S155 site in WDR24. **b**, In vitro GST–WDR24 kinase assays were performed, which revealed S155 as the main AMPK phosphorylation site of WDR24. The GST–WDR24 WT protein and S155A mutant were bacterially purified as substrates, and recombinant active AMPK was used as the source of kinase. Antibody against thiophosphate ester was used to detect phosphorylated proteins. **c**, *WDR24* KO HEK 293 cells reintroduced with the indicated constructs were deprived of Glc for 60 min and restimulated with Glc for 10 min as indicated. **d**, IB analysis of WCLs and anti-FLAG immunoprecipitates derived from *WDR24* knockout HEK 293 cells reconstituted with empty vector or WT WDR24. The resulting cells were further treated with the AMPK agonist A-769662 (100 μM) or 991 (40 μM) for 1 h before collection for IP and IB analyses. **e**, IB analysis of WCLs and anti-FLAG immunoprecipitates derived from WT or *AMPKα1/2* DKO FLAG–WDR24 knock-in (KI) HEK 293 cells. The resulting cells were deprived of Glc for 60 min and restimulated with Glc for 10 min as indicated. Representative image shown. In **b,d**, *n* = 2. In **c,e**, *n* = 3.
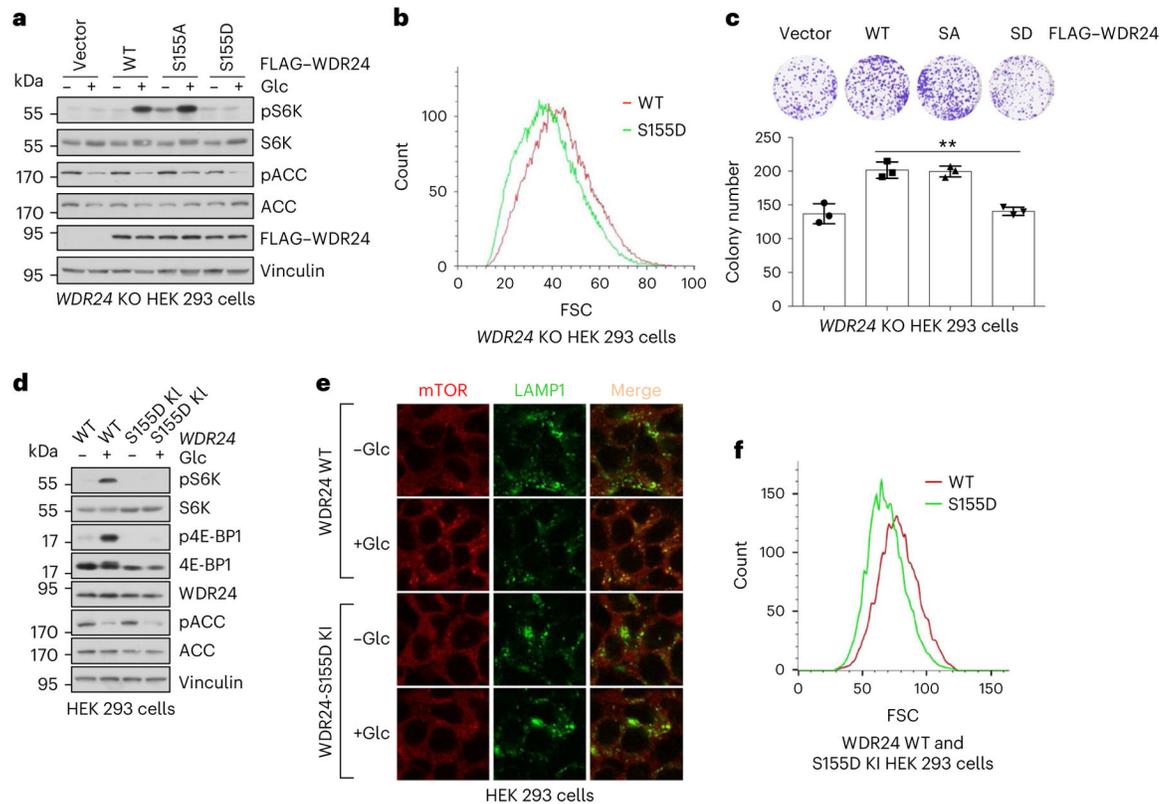
Fig. 4 |. AMPK-mediated phosphorylation of WDR24 on S155 regulates mTORC1 kinase activity.

a, *WDR24* KO HEK 293 cells reconstituted with the indicated constructs were deprived of Glc for 60 min and restimulated with Glc for 10 min as indicated. Representative image shown. $n = 2$. **b**, Cell size histogram of *WDR24* KO HEK 293 cells reconstituted with WT and WDR24-S155D analysed by flow cytometry. FSC, forward scatter. **c**, *WDR24* KO HEK 293 cells reconstituted with the indicated constructs were plated for the colony formation assays. Bottom, data are the mean ± s.d. of $n = 3$ independent experiments. $P = 0.001$, two-tailed *t*-test. **$P < 0.01$. **d**, WT and *WDR24-S155D* KI HEK 293 cells were deprived of Glc for 60 min and restimulated with Glc for 10 min as indicated. Representative image shown. $n = 3$. **e**, WT and *WDR24-S155D* KI HEK 293 cells were deprived of Glc for 60 min and restimulated with Glc for 10 min before immunostaining for mTOR (red) and LAMP1 (green). Scale bar, 10 μm. **f**, Cell size histogram of WT and *WDR24-S155D* KI HEK 293 cells analysed by flow cytometry.
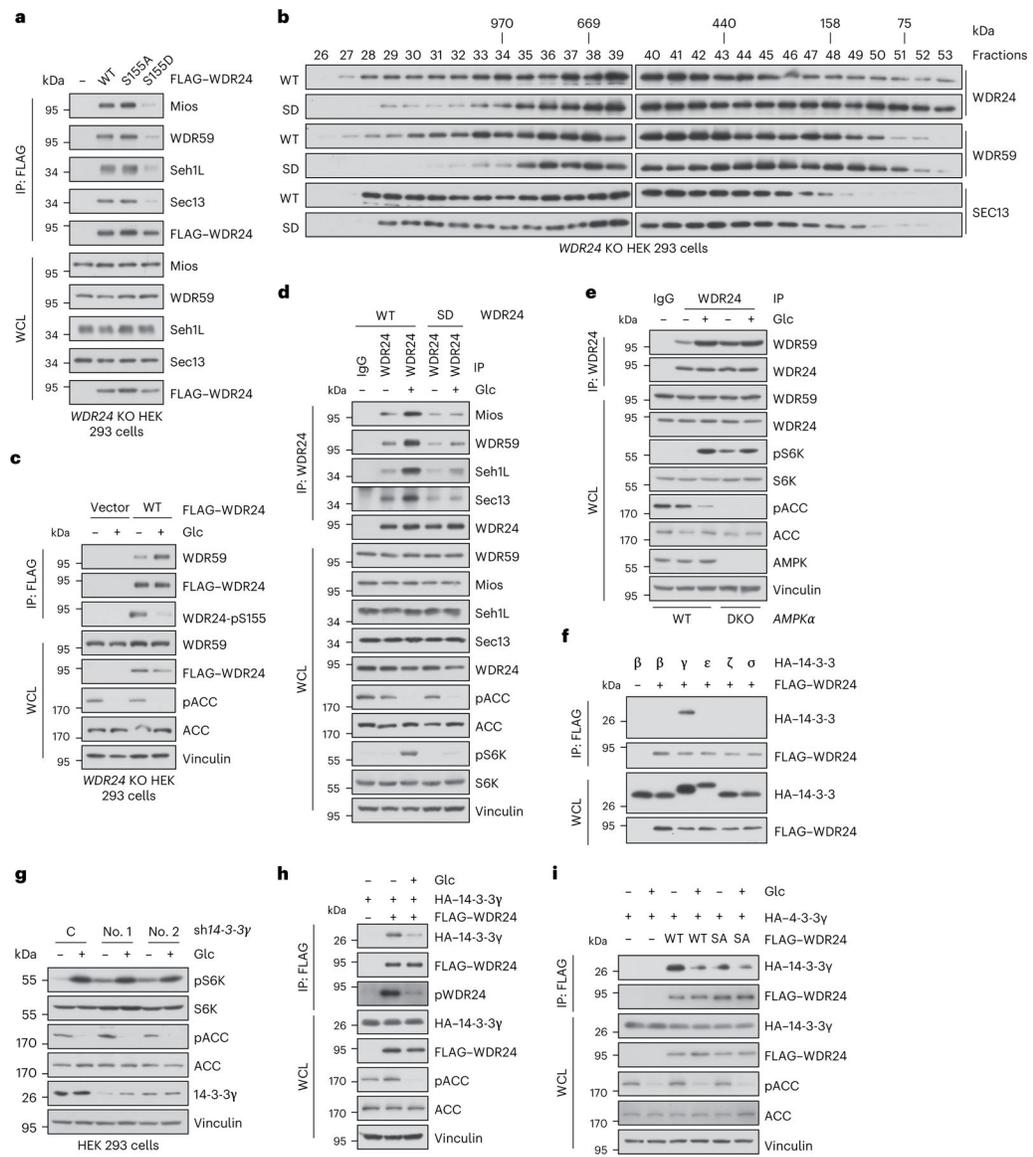
Fig. 5 |. Glucose regulates GATOR2 complex integrity through phosphorylation of WDR24 on S155.

a, IB analysis of WCLs and anti-FLAG immunoprecipitates derived from *WDR24* KO HEK 293 cells reconstituted with the indicated constructs. **b**, The WCLs of *WDR24* KO HEK 293 cells reconstituted with WT WDR24 or the S155D mutant were run through a Superose 6 Increase 10/300 GL column. Eluates were collected for each fraction and analysed by IB. **c**, IB analysis of WCLs and anti-FLAG immunoprecipitates derived from *WDR24* KO HEK 293 cells reconstituted with the indicated constructs. Cells were deprived of Glc for 60 min and restimulated with Glc for 10 min as indicated. **d**, IB analysis of WCLs and anti-WDR24 immunoprecipitates derived from WT and *WDR24-S155D* KI HEK 293 cells. Cells were treated as in **c**. **e**, IB analysis of WCLs and anti-WDR24 immunoprecipitates derived from WT and *AMPKα1/2* DKO HEK 293T cells reconstituted with the indicated constructs. Cells were treated as in **c**. **f**, IB analysis of WCLs and immunoprecipitates derived from HEK 293T cells transfected with the indicated constructs. **g**, WT and *14-3-3γ* KO HEK 293 cells

were deprived of Glc for 60 min and restimulated with Glc for 10 min as indicated. C, control. **h,i**, IB analysis of WCLs and immunoprecipitates derived from HEK 293T cells transfected with the indicated plasmids. The resulting cells were deprived of Glc for 60 min and restimulated with Glc for 10 min as indicated. Representative image shown. In **a,c,e,g–i**, $n = 3$. In **b,d,f**, $n = 2$.
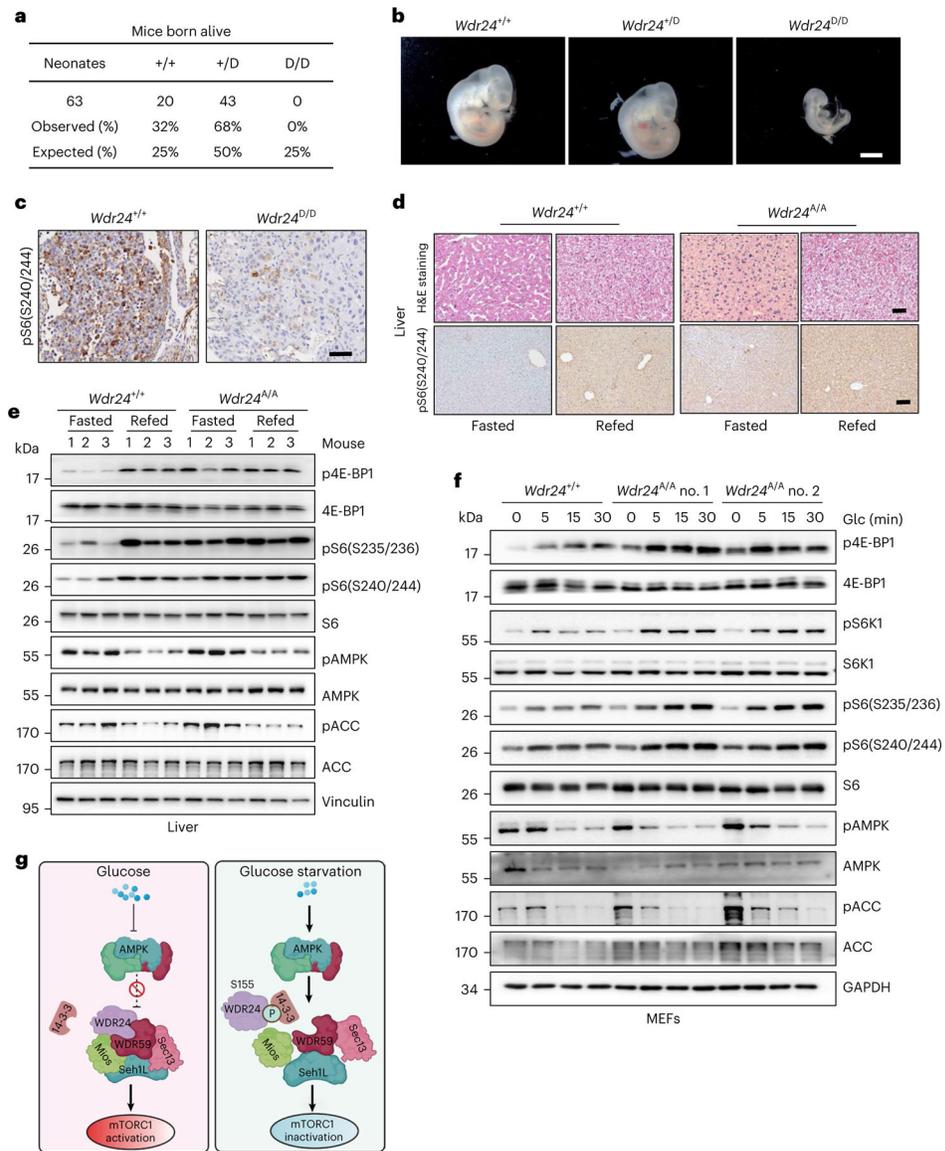
Fig. 6 |. WDR24 phosphorylation suppresses mTORC1 kinase activity and leads to embryonic lethality in vivo.

a, Neonates from *WDR24*[+/D] parents were counted at birth. **b**, Representative images of *Wdr24*^{+/+}, *Wdr24*[+/D] and *Wdr24*[D/D] embryos at embryonic day 10.5. Scale bar, 1 mm. **c**, Representative images of pS6(S240/244) staining of the liver section ($n = 3$) of *Wdr24*^{+/+} and *Wdr24*[D/D] littermates. Scale bar, 50 μm. **d**, Representative images of H&E (scale bar, 50 μm) and pS6(S240/244) staining (scale bar, 100 μm) of liver sections ($n = 3$) of *Wdr24*^{+/+} and *Wdr24*[A/A] littermates. Mice were fasted for 24 h or fasted and refed for 2 h. **e**, IB analysis of WCLs derived from *Wdr24*^{+/+} or *Wdr24*[A/A] mouse livers. Mice were fasted for 24 h or fasted and refed for 2 h. $n = 3$ mice. **f**, IB analysis of WCLs derived from *Wdr24*^{+/+} or *Wdr24*[A/A] MEFs. Cells were deprived of Glc for 60 min and restimulated with Glc for different time periods as indicated. $n = 2$ clones. **g**, Working model showing how glucose regulates mTORC1 kinase activity through AMPK-mediated WDR24 phosphorylation.